

THESIS

SECONDARY ORGANIC AEROSOL FORMATION FROM VOLATILE  
CHEMICAL PRODUCT EMISSIONS: PARAMETERS AND  
CONTRIBUTIONS TO ANTHROPOGENIC AEROSOL

Submitted by

Sreejith Sasidharan

Department of Mechanical Engineering

In partial fulfillment of the requirements

For the Degree of Master of Science

Colorado State University

Fort Collins, Colorado

Spring 2023

Master's Committee:

Advisor: Shantanu Jathar

John Volckens

Jeffrey Pierce

Copyright by Sreejith Sasidharan 2023

All Rights Reserved

## ABSTRACT

### SECONDARY ORGANIC AEROSOL FORMATION FROM VOLATILE CHEMICAL PRODUCT EMISSIONS: PARAMETERS AND CONTRIBUTIONS TO ANTHROPOGENIC AEROSOL

Volatile chemical products (VCP) are an increasingly important source of hydrocarbon and oxygenated volatile organic compound (OVOC) emissions to the atmosphere and these emissions are likely to play an important role as anthropogenic precursors for secondary organic aerosol (SOA). While the SOA from VCP hydrocarbons is often accounted for in ambient air quality models, the formation, evolution, and properties of SOA from VCP OVOCs remains uncertain. We use environmental chamber data and a kinetic model to develop SOA parameters for ten OVOCs representing glycols, glycol ethers, esters, oxygenated aromatics, and amines. Model simulations suggest that the SOA mass yields for these OVOCs are on the same magnitude as widely studied SOA precursors (e.g., long-chain alkanes, monoterpenes, and single-ring aromatics) and these yields exhibit a linear correlation with the difference between the carbon and oxygen numbers of the precursor. When combined with emissions inventories for two megacities in the United States (US) and a US-wide inventory, we find that VCPs form 0.8-2.5× as much SOA, by mass, as mobile sources. Hydrocarbons (terpenes, branched and cyclic alkanes) and OVOCs (terpenoids, glycols, glycol ethers) make up 60-75% and 25-40% of the SOA arising from

VCP use, respectively. This work contributes to the growing body of knowledge focused on studying VCP VOC contributions to urban air pollution.

## ACKNOWLEDGEMENTS

I would first like to thank Dr. Shantanu Jathar for being a fantastic advisor, and for supporting me throughout my graduate studies. I would also like to extend my gratitude to Dr. John Volckens and Dr. Jeffrey Pierce for their invaluable inputs during the course of my studies.

## TABLE OF CONTENTS

ABSTRACT.....	ii
ACKNOWLEDGEMENTS.....	iv
Chapter 1: Introduction.....	1
Chapter 2: Materials & Methods.....	5
Chapter 3: Results.....	16
References.....	35
Supplementary Information.....	40

## CHAPTER 1 - INTRODUCTION

Volatile chemical products (VCPs), which include personal care products, cleaning agents, paints, coatings, printing inks, adhesives, and pesticides, have recently been highlighted as an important source of volatile organic compound (VOC) emissions to the atmosphere.<sup>1</sup> In the United States (US)<sup>2</sup> their emissions (3 to 7 Tg yr<sup>-1</sup>) are likely to rival VOC emissions from more traditional sources such as mobile sources (2.7 to 3.5 Tg yr<sup>-1</sup>) and oil and natural gas production activities (up to 5.7 Tg yr<sup>-1</sup>).<sup>2,3</sup> VCP VOCs can participate in photochemical reactions to produce secondary organic aerosol (SOA) and ozone (O<sub>3</sub>). Several studies now suggest that VCP use is an important contributor to both anthropogenic SOA and O<sub>3</sub> in urban environments, especially in densely populated regions.<sup>4-10</sup> SOA makes up a significant fraction of PM<sub>2.5</sub> (mass of particles smaller than 2.5 μm), and together with O<sub>3</sub>, are important constituents of poor air quality. Despite recognition of the potential role of VCP use on air quality, it remains one of the most uncertain sources of air pollution in US cities.

VCP emissions are understood to be composed of both hydrocarbons and oxygenated VOCs. VCP hydrocarbons include organic classes such as linear, branched, and cyclic alkanes, single- and multi-ring aromatics, and acyclic (e.g., linear and branched) and cyclic (e.g., monoterpenes) alkenes.<sup>6,7,11</sup> Over the past several decades, an extensive body of work has attempted to understand mass yields, composition, and properties of SOA formed from alkane (e.g., Lim and Ziemann;<sup>12</sup> Presto et al.<sup>13</sup>), alkene (e.g., Ng et al.;<sup>14</sup> Paulot et al.<sup>15</sup>), and aromatic (e.g., Ng et al.,<sup>16</sup> Li et al.<sup>17</sup>) hydrocarbons and these compound classes are represented in three-dimensional chemical transport models (CTMs; e.g., Qin et al.<sup>4</sup>). As a result, VCP hydrocarbon emission impacts on atmospheric chemistry and air quality can be simulated.

In contrast, the composition, oxidation chemistry, and potential to form SOA and O<sub>3</sub> for VCP Oxygenated Volatile organic compounds (OVOCs) is less well understood. VCP OVOCs belong to a wide variety of organic compound classes. Those emitted in substantial amounts, as estimated in previous efforts,<sup>1,6,11</sup> include glycols, glycol ethers, siloxanes, esters, acetates, oxygenated aromatics, and heterocyclics. Recently, some of these organic classes have been studied in the laboratory for their ability to produce SOA. For instance, Li et al.<sup>18</sup> performed environmental chamber experiments to study SOA formation from a survey of VCP OVOCs under high NO<sub>x</sub> conditions and found certain glycol ethers (e.g., carbitol and butyl carbitol), oxygenated aromatics (e.g., benzyl alcohol), and large acetates (e.g., dipropylene glycol methyl ether acetate) to produce SOA efficiently, with mass yields that ranged between 10 and 55%. Charan et al.<sup>19</sup> performed a comprehensive set of chamber experiments with benzyl alcohol and, consistent with Li et al.,<sup>18</sup> measured very high SOA mass yields (35-104%), noting that these were calculated at very high OA mass loadings (100-600 μg m<sup>-3</sup>). Using an oxidation flow reactor (OFR), Humes et al.<sup>20</sup> studied SOA formation from select glycol ethers, esters, and oxygenated aromatics but only found the cyclic OVOCs (i.e., oxygenated aromatics) to form any SOA (average yield of 16%), with near zero SOA mass yields for acyclic OVOCs (i.e., glycol ethers, esters).

Several studies have performed flow reactor experiments with decamethylcyclopentasiloxane (D5), a common ingredient found in personal care products.<sup>22,24-26</sup> Although there were large differences in the reported SOA formation between these studies, they all estimated high SOA mass yields for D5 under high OH exposures (ranging from 5 to 100% for >18 hours of photochemical age). However, when Charan et al.<sup>26</sup> studied D5 in chamber experiments over shorter photochemical ages (<12 hours), D5 seemed to produce little to no SOA

(mass yields <1%). In general, the body of literature focused on SOA formation from VCP OVOCs is small and uncertain, relative to that for VCP hydrocarbons.

Laboratory experiments performed with chambers and flow reactors have historically provided the underlying data needed to develop chemical mechanisms and parameterizations for SOA for use in CTMs.<sup>68</sup> Yet, both chambers and flow reactors are subject to experimental artifacts,<sup>44</sup> some of which can be corrected for empirically (e.g., particle wall losses<sup>69</sup>) but others (e.g., vapor wall losses,<sup>70</sup> short timescales for oxidation in flow reactors<sup>71</sup>) require use of kinetic models to help with interpretation of the laboratory data. For instance, He et al.<sup>32</sup> showed that a careful accounting of aerosol processes (e.g., gas-phase chemistry, gas/particle partitioning, wall losses, condensed-phase chemistry, phase state) using a kinetic model helped explain observed differences in SOA formation between chambers and flow reactors from photooxidation of  $\alpha$ -pinene. Few, if any, SOA parameters have been developed from laboratory data for VCP OVOCs, but any future parameter development should aim to use process-based kinetic models.

Several studies so far have simulated urban air quality impacts from VCP emissions and all have found VCP VOCs to play a key role in influencing the urban SOA burden.<sup>4,9,10</sup> Qin et al.<sup>4</sup> used a bulk SOA mass yield to model SOA formation from VCPs to show that VCP VOCs might account for ~40% of the anthropogenic SOA in Los Angeles in the summer. Seltzer et al.<sup>11</sup> developed a detailed nationwide emissions inventory for VCP VOCs by county that accounted for speciated formulations by product use category while also considering timescales for use and evaporation. Pennington et al.<sup>9</sup> introduced two new precursors and leveraged six hydrocarbon-like precursor classes<sup>21</sup> developed for mobile sources to simulate the oxidation chemistry and SOA formation from oxygenated and non-oxygenated VCP VOCs. Based on the updated inventory and chemistry scheme, Seltzer et al.<sup>10</sup> found that VCPs contributed to 20% of the seasonal

anthropogenic SOA in Los Angeles (and New York City) and Pennington et al.<sup>9</sup> showed that up to ~50% of the midday anthropogenic SOA could arise from VCP use. Regardless, all three previous modeling studies have relied on simplified approaches to simulate SOA formation from VCP OVOCs. Although laboratory data for VCP OVOCs are currently limited to only a handful of studies,<sup>18–20,22–26</sup> these data are generally not used to parameterize SOA in CTMs.

In this work, we combined environmental chamber data from Li et al.<sup>18</sup> and a kinetic chemistry-microphysics model to simulate SOA formation from a representative set of VCP-related OVOCs. The kinetic model was used to estimate atmospherically relevant SOA mass yields and develop volatility basis set (VBS) parameters for a diversity of VCP OVOCs. These were subsequently used to calculate the contribution of total VCP use and the most important VCP hydrocarbons and OVOCs to anthropogenic SOA, relative to fossil fuel combustion.

## CHAPTER 2 - MATERIALS & METHODS

### *2.1 SOA Environmental Chamber Data*

The SOA parameters developed and applied in this work are based on the environmental chamber data reported in Li et al.<sup>18</sup> Li et al.<sup>18</sup> performed chamber experiments on fourteen unique VCP OVOCs, with a minimum of one experiment performed for each OVOC and several perturbations performed for a few select OVOCs. Li et al.<sup>18</sup> chose those OVOCs because they are widely used to produce and/or are directly present in industrial solvents, cleaning and personal care products, paints and coatings, adhesives, and printing inks. We focus our efforts on SOA data from thirteen experiments performed on ten OVOCs for which complete gas, particle, and environmental data were available to perform the modeling. The OVOCs, in increasing carbon number, are: propylene glycol, diethylene glycol, carbitol (diethylene glycol ethyl ether), triethanolamine, benzyl alcohol, dimethyl glutarate, butyl carbitol (diethylene glycol monobutyl ether), dipropylene glycol methyl ether acetate (DPGMEA), Texanol (2,2,4-trimethyl-1,3-pentanediol monoisobutyrate), and methyl palmitate. Triethanolamine, though it contains an N atom, would be classified as an OVOC. A brief description of the chamber experiments is provided below, but the reader is referred to Li et al.<sup>18</sup> for more details.

The SOA experiments were performed in the dual indoor environmental chamber facility located at the University of California, Riverside (UCR);<sup>28</sup> the SOA data are summarized in Tables 1 and S1. The Teflon chambers each had a volume of 30 m<sup>3</sup> and were located in a temperature- and humidity-controlled enclosure. Before starting each experiment, the chambers were cleaned by reducing the chamber volume to less than 5% of its original volume, while flushing the chamber with zero air. The chambers were subsequently filled to capacity with zero air. NO and NO<sub>2</sub>

(generated in-situ via chemical conversion of NO) were directly added to achieve concentrations of ~20 ppbv and ~10 ppbv, respectively.

Table 1: Summary of data for the high NO<sub>x</sub> chamber experiments performed by Li et al.<sup>18</sup> and those used in this work to develop SOA parameters.

VCP OVOC	Formula	MW (g.mole <sup>-1</sup> )	k <sub>OH</sub> (cm <sup>3</sup> molec <sup>-1</sup> s <sup>-1</sup> )	Seed (μm <sup>2</sup> cm <sup>-3</sup> )	Surrogate VOC Mix.?	H <sub>2</sub> O <sub>2</sub> Added	Initial VOC <sub>0</sub> (ppbv)	Initial NO (ppbv)	Initial NO <sub>2</sub> (ppbv)	OH Exposure (molec. hr cm <sup>-3</sup> )	Max. SOA (μg m <sup>-3</sup> )	SOA Mass Yield (Max.)	SOA O:C
Propylene glycol	C <sub>3</sub> H <sub>8</sub> O <sub>2</sub>	76.09	2.15×10 <sup>-11</sup>	NA	Y	N	40	19	9.0	7.1×10 <sup>6</sup>	3.59	0.07	0.55 <sup>&amp;</sup>
Diethylene glycol	C <sub>4</sub> H <sub>10</sub> O <sub>3</sub>	106.12	2.75×10 <sup>-11</sup>	NA	Y	N	80	21	8.7	1.4×10 <sup>7</sup>	2.27	0.01	NM
Carbitol	C <sub>6</sub> H <sub>14</sub> O <sub>3</sub>	134.17	5.16×10 <sup>-11</sup>	NA	Y	N	40	20	12	8.3×10 <sup>6</sup>	22.71	0.13	0.6-1.2 <sup>&amp;</sup>
Triethanolamine	C <sub>6</sub> H <sub>15</sub> NO <sub>3</sub>	149.18	1.11×10 <sup>-10</sup>	1080	Y	N	40	22	14	5.4×10 <sup>6</sup>	3.57	0.02	NM
Benzyl Alcohol	C <sub>7</sub> H <sub>8</sub> O <sub>1</sub>	108.13	2.80×10 <sup>-11</sup>	2334	N	Y	79	71	-	4.9×10 <sup>7</sup>	171.0	0.49	0.8-0.86 <sup>&amp;</sup>
Dimethyl Glutarate	C <sub>7</sub> H <sub>12</sub> O <sub>4</sub>	160.16	3.50×10 <sup>-12</sup>	185	N	Y	160	12	12	4.4×10 <sup>7</sup>	4.50	0.01	0.72
Butyl Carbitol	C <sub>8</sub> H <sub>18</sub> O <sub>3</sub>	162.22	7.44×10 <sup>-11</sup>	NA	Y	Y	40	18	9.8	9.7×10 <sup>6</sup>	67.64	0.28	0.98
Dipropylene Glycol Methyl Ether Acetate (DPGMEA)	C <sub>9</sub> H <sub>18</sub> O <sub>4</sub>	190.24	3.36×10 <sup>-11</sup>	NA	Y	Y	40	12	6.8	2.8×10 <sup>7</sup>	78.53	0.26	0.17

Texanol	$C_{12}H_{24}O_3$	216.31	$1.29 \times 10^{-11}$	NA	Y	N	80	18	10	$8.9 \times 10^6$	1.07	0.004	0.34
Methyl Palmitate	$C_{17}H_{34}O_2$	270.45	$1.88 \times 10^{-11}$	287	Y	N	40	21	6.9	$1.7 \times 10^7$	177.99	0.60	NM

*&Measurement based on a different experiment; NA=unseeded experiment; NM=not measured.*

The NO<sub>x</sub> values reported in this table are comparable to that observed in major cities worldwide. As an example, the mean NO<sub>x</sub> concentrations at the Caltech supersite for the period May 27 – June 15, 2010 has been shown to be ~21.8 ppbv.<sup>72</sup> Similarly, the NO<sub>2</sub> levels in Beijing have been reported to be ~ 21 ppbv. A surrogate hydrocarbon mixture (22.6 of *m*-xylene, 98.7 of *n*-butane, 22.7 of *n*-octane, 14.9 of trans-2-butene, 25.4 of toluene, 17.9 of ethylene, and 14.9 of propylene; units of ppbv) was added in eight of the ten experiments to mimic urban atmospheric conditions.<sup>28</sup> Approximately 1 ppmv of hydrogen peroxide (H<sub>2</sub>O<sub>2</sub>) was added in four of the ten experiments, photolysis of which resulted in elevated concentrations of hydroxyl radicals (OH); OH was produced in the other six experiments from VOC-NO<sub>x</sub> chemistry. Ammonium sulfate seed was added in four of the ten experiments to facilitate SOA condensation on the pre-existing seed; SOA was allowed to homogeneously nucleate in the other six experiments. Despite seed addition, there was evidence for nucleation in the experiment performed with methyl palmitate. Constituents in both chambers were then mixed together to achieve uniform concentrations in both chambers before they were separated again. The VCP OVOC of interest was only added to one of the chambers, with the other chamber serving as a control. The initial OVOC concentrations ranged from 40 to 160 ppbv. 272 UV black lights with a net rated NO<sub>2</sub> photolysis rate of 0.4 min<sup>-1</sup> were turned on to initiate photo-oxidation.

A suite of instrumentation was used to measure gas phase mixing ratios, aerosol mass concentrations and composition, and environmental conditions in both chambers. NO, NO<sub>2</sub>, and O<sub>3</sub> were measured using standard gas analyzers, and the VCP OVOCs were monitored either using gas chromatography or mass spectrometry. The measured decay of *m*-xylene (in cases where a surrogate mixture was added) or the OVOC (when no surrogate mixture was used) was used to quantify OH concentrations and exposure during the chamber experiment. Particle size

distributions and mass concentrations were quantified using a combination of a scanning mobility particle sizer (SMPS), aerosol particle mass analyzer (APM) coupled to an SMPS, and a high-resolution aerosol mass spectrometer (HR-AMS). The Teflon walls had little to no observed influence on the parent OVOC mixing ratios, and hence no corrections were needed. VOC oxidation products are subject to losses on Teflon walls and these were accounted for in the kinetic model (explained later). The particle data were corrected for losses of particles to the wall, following the methods described in Cocker et al.,<sup>27</sup> as well as corrected for any SOA production from the surrogate mixture in the control chamber. As the aerosol mass spectrometer only sampled from the chamber with OVOC added, the SOA O:C data were not corrected for the SOA produced from the surrogate mixture.

## ***2.2 SOM-TOMAS Model, Simulations, and SOA Parameters***

We used the SOM-TOMAS model, or Statistical Oxidation Model (SOM)-Two Moment Aerosol Sectional (TOMAS) model, to simulate the SOA formation and composition from photooxidation of the ten OVOCs mentioned earlier. SOM uses a two-dimensional carbon-oxygen grid to simulate the multiphase and multigenerational oxidation chemistry of VOCs and calculates the thermodynamic properties of the oxidation products.<sup>29</sup> TOMAS uses a number and mass moment scheme to simulate aerosol processes of coagulation, condensation, evaporation, and nucleation.<sup>30</sup> A detailed description of the SOM-TOMAS model along with the governing equations can be found in previous publications.<sup>31,32</sup> Recently, the SOM-TOMAS model was used to study SOA formation from biomass burning emissions and evaporated biofuels in chamber experiments,<sup>31,33</sup> from  $\alpha$ -pinene in an oxidation flow reactor,<sup>32</sup> inside wildfire plumes,<sup>34</sup> and at a continental rural site.<sup>67</sup>

The SOM-TOMAS is a parameterized model and uses the following five parameters to track the oxidation chemistry of the VOC and its oxidation products that includes both

functionalization and fragmentation reactions: (i-iv)  $p_{f,1}$  to  $p_{f,4}$ , mass yields for four functionalized products that add one, two, three, and four oxygen atoms to the carbon backbone, respectively; and (v)  $m_{frag}$ , a parameter used to calculate the probability of fragmentation ( $P_{frag}$ ) based on the oxygen-to-carbon ratio (O:C) of the model species ( $P_{frag} = (O:C)^{m_{frag}}$ ). A sixth parameter,  $\Delta LVP$  that quantifies the decrease in volatility with the addition of an oxygen atom, is used to calculate the volatility ( $c^*$ ) of the model species. The reaction rate constant of the model species with OH is parameterized as a function of its carbon ( $N_C$ ) and oxygen ( $N_O$ ) number. SOM-TOMAS uses a diffusive-reactive framework to simulate kinetic gas/particle partitioning of condensable model species, subject to the prescribed phase state of the absorbing organic aerosol.<sup>35</sup> Finally, vapor losses to the chamber walls are modeled using the framework presented in Matsunaga and Ziemann<sup>36</sup> and Krechmer et al.<sup>37</sup> where the first-order uptake to the walls is assumed to be equal to  $k_{vap,on}$  and the release of vapors from the walls ( $k_{vap,on}$ ) is modeled using absorptive partitioning theory with the Teflon wall serving as an absorbing mass with an effective mass concentration of  $C_w \text{ mg m}^{-3}$ . Vapor wall loss has not been specifically studied for the UCR chamber, so  $k_{vap,on}$  is assumed to be equal to  $2.5 \times 10^{-4} \text{ s}^{-1}$  based on the work of Zhang et al.<sup>38</sup> for a  $30 \text{ m}^3$  chamber.

In addition, SOM-TOMAS can simulate autoxidation (e.g., Ehn et al.<sup>39</sup>), reactive uptake (e.g., Shiraiwa et al.<sup>40</sup>), and oligomerization (e.g., D'Ambro et al.<sup>41</sup>) reactions, some of which have recently been shown to be influential for SOA formation from photooxidation of  $\alpha$ -pinene.<sup>32</sup> However, in the absence of dedicated measurements for the OVOCs studied here, the relative importance of these processes remains uncertain and, hence, these processes were not considered in this work. Finally, SOM-TOMAS can also simulate heterogeneous oxidation via OH, but these reactions were found to have limited influence on SOA formation (not shown), likely due to the

short photochemical ages encountered in the chamber experiments (3.6 to 33 hours at an OH concentration of  $1.5 \times 10^6$  molecules  $\text{cm}^{-3}$ ).

The SOM-TOMAS model was initialized with the VOC mixing ratio, seed particle size distribution (in cases where ammonium sulfate seed was injected), and the environmental conditions (i.e., temperature, relative humidity). In experiments where SOA homogeneously nucleated, observations of the total particle number concentration were used to develop an empirical parameterization for the nucleation rate, which was then fed to the model (see Figure S1). The time-varying OH concentrations, obtained from the *m*-xylene or OVOC decay, were directly prescribed in the model. As the SOA data were already corrected for data from the control chamber, we did not simulate SOA formation from the surrogate mixture.

The SOM-TOMAS model was used to determine SOA parameters ( $p_{f,1}$  to  $p_{f,4}$ ,  $m_{\text{frag}}$ ,  $\Delta LVP$ ) for each OVOC studied in this work by fitting model predictions of SOA mass concentrations to the observations. Initial guesses for the SOA parameters were varied randomly before arriving at the final set of fit parameters. We fit model predictions to the mean observations of SOA, which are expected to carry a minimum uncertainty of 38% (at the 95% confidence interval, based on Bahreini et al.<sup>42</sup>). By extension, model predictions based on those SOA parameters also carry a minimum uncertainty of 38%. In previous work, we have determined SOA parameters by simultaneously fitting observations of SOA mass concentrations and O:C.<sup>33</sup> However, time series data for O:C were available for only four of the OVOC experiments and, for three of these experiments, the O:C data were not corrected for SOA produced from the surrogate mixture. Hence, we did not include O:C data within the fitting procedure. For select OVOCs, the SOM-TOMAS model was run with the fit parameters for repeat experiments performed with the same OVOC to evaluate those SOA parameters (Table S1).

### ***2.3 VBS<sub>SOM</sub> Model and Parameters***

The SOM-TOMAS model output was used to develop VBS (or VBS<sub>SOM</sub>) parameters for VCP OVOCs that theoretically account for the influence of multigenerational aging and some of the important environmental chamber artifacts (i.e., particle and vapor wall losses). This approach was identical to that developed by our group to develop VBS parameters for SOA precursors in a widely used CTM (GEOS-Chem) and more details can be found in Bilsback et al.<sup>43</sup> Briefly, we performed pseudo atmospheric simulations with the SOM-TOMAS model for 48 hours (2 days) at three different OA mass concentrations (0.1, 1, and 10  $\mu\text{g m}^{-3}$ ) and an OH concentration of  $1.5 \times 10^6$  molecules  $\text{cm}^{-3}$ . The simulation length of 48 hours was chosen to capture the SOA production that might occur within the atmospheric envelope of a large city. As will be shown later, the SOA mass yields predicted by the SOM-TOMAS model seem to level off for most OVOCs past 48 hours of photochemical aging. The OA mass loadings, and OH concentrations were chosen to ensure that the VBS<sub>SOM</sub> parameters were atmospherically relevant.<sup>44</sup> The SOM-TOMAS predictions of SOA mass yields with time were fit to determine VBS<sub>SOM</sub> parameters, separately for each OVOC. We chose to fit a ‘static’ set of VBS<sub>SOM</sub> parameters to keep the parameterization simple and consistent with how most modern VBS schemes are implemented in CTMs.<sup>21,45,46</sup> A limitation of this assumption is that the VBS<sub>SOM</sub> parameters will not be able to reproduce the time-varying SOA mass yield predicted by the SOM-TOMAS model, especially at short photochemical ages. The SOA mass yields and VBS<sub>SOM</sub> parameters determined in this exercise are likely to be upper bound estimates since we do not simulate losses of the VOC oxidation products to processes other than homogeneous gas-phase chemistry (e.g., dry and wet deposition, photolysis, surface chemistry).

#### ***2.4 SOA Production from VCPs and Mobile Sources***

SOA mass yields from the SOM-TOMAS atmospheric simulations were used to estimate SOA production from VOC emissions from mobile sources and VCP use. This analysis was

performed with three previously published VOC emissions inventories for VCPs for the following regions and years: South Coast Air Basin (SoCAB) in California for 2010 based on McDonald et al.,<sup>1</sup> New York City (NYC) in New York for 2018 based on Coggon et al.,<sup>6</sup> and US for 2017 based on Seltzer et al.<sup>11</sup> VOC emissions from mobile sources for SoCAB and NYC were based on the Fuel-based Inventory of motor-Vehicle Emissions (FIVE)<sup>47</sup> and those for the US were based on the National Emissions Inventory for 2017.<sup>48</sup> Annual estimates from these regions were normalized by the population to present VOC emissions and SOA production information on a kg person<sup>-1</sup> yr<sup>-1</sup> basis.

The three different VCP emissions inventories were based on combining inputs for total chemical product use, composition profiles, timescales for product use and evaporation, and spatial allocation by population. The level of classification and VOC speciation varied across these three inventories with the SoCAB inventory being less detailed (on account of being the first such dataset) and the NYC and US inventories being the most comprehensive (later efforts). For SoCAB and NYC, the emissions magnitudes for all VCP VOCs were further adjusted by constraining the estimated emissions ratios for select VOCs to corresponding measurements available from stationary sites (for SoCAB) or mobile monitoring efforts (for NYC).<sup>1,6</sup> No such adjustments were made for the US inventory.

Reaction rate constants for the VOCs with OH were based on values reported in the literature (e.g., Atkinson and Arey<sup>49</sup>) or from EPISuite v4.11.<sup>48</sup> To keep the SOA production estimates relevant for urban environments, the VOC reacted and SOA mass yields were calculated for a photochemical age of 12 hours (OH concentration of  $1.5 \times 10^6$  molecules cm<sup>-3</sup>);<sup>50</sup> SOA mass yields were based on an OA mass loading of 10  $\mu\text{g m}^{-3}$ . By selecting experiments with high NO concentrations, the SOA mass yields are reflective of RO<sub>2</sub>+NO dominant conditions with a

transition towards increasing  $\text{RO}_2+\text{HO}_2$  towards the end of experiments, typical of plumes from urban environments. The methods and assumptions used to calculate the SOA mass yields for OVOCs and hydrocarbons are described in Section S1 in the supporting information.

## CHAPTER 3 - RESULTS

### 3.1 SOA Formation from VCP OVOCs

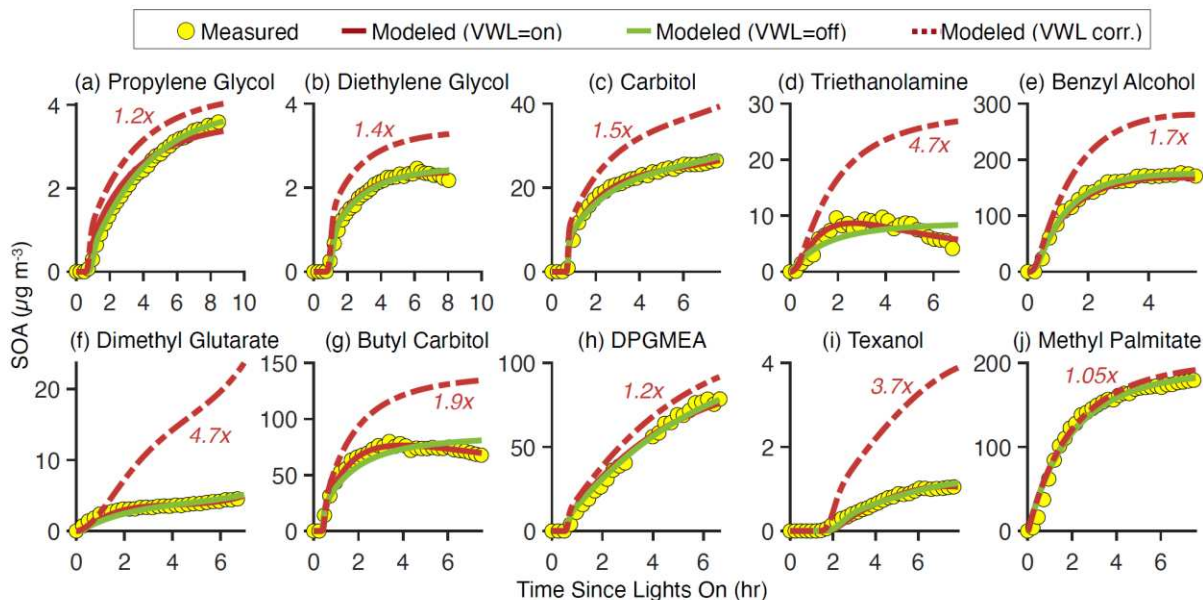


Figure 1: Predictions of SOA mass concentration from the SOM-TOMAS model compared to observations for ten different OVOCs. OVOCs are ordered by carbon number: (a) propylene glycol ( $C_3H_8O_2$ ), (b) diethylene glycol ( $C_4H_{10}O_3$ ), (c) carbitol ( $C_6H_{14}O_3$ ), (d) triethanolamine ( $C_6H_{15}NO_3$ ), (e) benzyl alcohol ( $C_7H_8O$ ), (f) dimethyl glutarate ( $C_7H_{12}O_4$ ), (g) butyl carbitol ( $C_8H_{18}O_3$ ), (h) dipropylene glycol methyl ether acetate (DPGMEA;  $C_9H_{18}O_4$ ), (i) Texanol ( $C_{12}H_{24}O_3$ ), and (j) methyl palmitate ( $C_{17}H_{34}O_2$ ). Predictions are shown in solid lines (dull red for VWL=on (corrected for vapor wall losses) and lime green for VWL=off (not corrected for vapor wall losses)) while observations are shown as symbols (yellow circles). The number labels ( $\#x$ ) describe the increase in SOA formation between the VWL=on and VWL=off simulations at the end of the experiment. SOA parameters (VWL=on and VWL=off) used with the SOM-TOMAS model for these OVOCs are listed in Table 2.

The SOM-TOMAS model was fit separately to observations of SOA mass concentrations for high  $NO_x$  experiments performed on ten different OVOCs to determine SOA parameters. Predictions based on the SOM-TOMAS fits are compared to observations in Figure 1 and the corresponding parameters for all ten OVOCs are listed in Table 2.

Table 2: SOM-TOMAS parameters based on fitting high NO<sub>x</sub> chamber data from Li et al.<sup>18</sup> for ten different OVOCs. Parameters are listed with (VWL=on) and without (VWL=off) considering vapor wall losses.

VCP OVOC	VWL	$\Delta LVP$	$m_{frag}$	$p_{r1}$	$p_{r2}$	$p_{r3}$	$p_{r4}$
Propylene Glycol	On	2.1092	0.2660	0.0014	0.5625	0.0001	0.4360
	Off	1.7994	0.4919	0.1772	0.0817	0.5881	0.1531
Diethylene Glycol	On	1.7130	0.1179	0.7253	0.0002	0.0501	0.2245
	Off	1.4731	0.0764	0.4773	0.0100	0.2142	0.2985
Carbitol	On	1.6346	0.4370	0.3119	0.4262	0.0013	0.2605
	Off	1.6163	0.3439	0.4489	0.0387	0.4984	0.0140
Triethanolamine	On	2.0778	0.1103	0.8841	0.1152	0.0000	0.0007
	Off	1.6520	0.0496	0.0040	0.0059	0.9576	0.0325
Benzyl Alcohol	On	1.1960	1.1260	0.0000	0.7780	0.0100	0.2110
	Off	1.1580	0.6470	0.0140	0.6020	0.0020	0.3820
Dimethyl Glutarate	On	1.4970	0.0360	0.6850	0.1530	0.1240	0.0380
	Off	1.2930	0.0380	0.0020	0.0130	0.3660	0.6190
Butyl Carbitol	On	1.0975	0.7268	0.0010	0.0000	0.9982	0.0008
	Off	1.2840	0.2990	0.0007	0.0012	0.5600	0.4381
DPGMEA	On	1.5861	0.6053	0.0005	0.0010	0.3254	0.6731
	Off	1.6796	0.5482	0.0003	0.0005	0.1927	0.8065
Texanol	On	1.0414	0.0200	0.4755	0.0037	0.4502	0.0706
	Off	1.0300	0.0080	0.6288	0.0089	0.0293	0.3331
Methyl Palmitate	On	2.1023	0.2687	0.0176	0.9456	0.0340	0.0028
	Off	1.3981	0.3492	0.9478	0.0316	0.0052	0.0153

Separate fits were developed with and without accounting for vapor wall losses (VWL=on and VWL=off, respectively) and both model configurations seemed to reproduce the SOA observations well. It should be noted that, these 6 SOM-TOMAS parameters aren't correlated in any way. In addition, it is possible to establish confidence intervals (CI) about the parameter fits. It is dependent on the scatter in the measured data, that the model is fit to. We note that the SOA mass concentration data were already corrected for particle wall losses.<sup>18</sup> There were two experiments (triethanolamine and butyl carbitol) where the model configuration with VWL=on did better than the model configuration with VWL=off. Here, the model configuration with VWL=on was able to reproduce the slight decline in SOA mass concentrations after 3 hours of photochemical aging. The decrease in the observed SOA mass concentrations with time could result from a host of reasons including, but not limited to, the use of an imprecise particle wall loss rate that might be changing with time<sup>51</sup> or losses of semi-volatile vapors to photolysis<sup>52</sup> or fragmentation<sup>53</sup> reactions. The SOM-TOMAS fits listed in Table 2 were found to be robust in that they did not vary significantly when the fitting procedure used different initial guesses for the SOA parameters. For the relatively short photochemical exposures encountered in the chamber experiments (3.6 to 33 equivalent hours at an OH concentration of  $1.5 \times 10^6$  molecules  $\text{cm}^{-3}$ ), heterogeneous oxidation with OH did not seem to have a meaningful effect on either the SOA mass concentration or O:C predictions (not shown), consistent with He et al.<sup>32</sup> Overall, the quality of the model-measurement comparisons was similar to that observed in earlier work with the SOM-TOMAS model and environmental chamber data.<sup>31-33,54</sup>

When the SOM-TOMAS model was re-run with the fit parameters corrected for vapor wall losses (VWL=on) but with vapor wall losses turned off during the chamber simulation to mimic ambient conditions, the model predicted an increase in SOA mass concentrations. For seven

OVOCs, the SOA production increased between 5% (methyl palmitate) and 90% (butyl carbitol), which was reasonably consistent with the increase in SOA production estimated for alkane, aromatic, and biogenic VOCs for chambers between 10 and 30 m<sup>3</sup> under high NO<sub>x</sub> conditions.<sup>33,38</sup> In contrast, the increase in SOA production was quite large for the three remaining OVOCs (factors of 3.7, 4.7, and 4.7 for Texanol, triethanolamine, and dimethyl glutarate, respectively), the primary reason for which can be explained as follows. These three OVOCs (i.e., Texanol, triethanolamine, and dimethyl glutarate) had much smaller SOA mass yields (0.004-0.02; see Table 1) compared to six of the other remaining OVOCs (0.07-0.60; see Table 1); results for diethylene glycol remained an exception. A smaller observed SOA mass yield meant that most of the OVOC oxidation products were left in the gas phase and subjected to vapor wall losses. The OVOC oxidation products, which were lost to the chamber walls during the experiment, had some residual potential to form SOA. So, when the SOM-TOMAS model was run with VWL turned off, it predicted a much larger increase in SOA production for these three OVOCs, relative to the effect observed for the six remaining OVOCs that had higher SOA mass yields. In essence, we are implying that when the SOM-TOMAS model is constrained to chamber data it is very likely to produce a large VWL effect for precursors that are not very efficient in producing SOA (say, SOA mass yields less than 2% in these experiments), everything else being equal. Previously, several chamber studies have been able to constrain the VWL effect by performing experiments under varying initial seed surface area concentrations or condensational sinks.<sup>19,38,55</sup> A similar set of experiments might need to be performed to better understand the VWL effect for individual OVOCs and the SOM-TOMAS-informed VWL-corrected SOA estimates in this work need to be considered with caution.

The SOA parameters determined from fitting one set of experiments were evaluated by comparing SOM-TOMAS model predictions based on those parameters against observations from a different experiment performed on the same OVOC. Results for propylene glycol, diethylene glycol, and carbitol, OVOCs for which repeat experimental data were available, are presented in Figure 2.

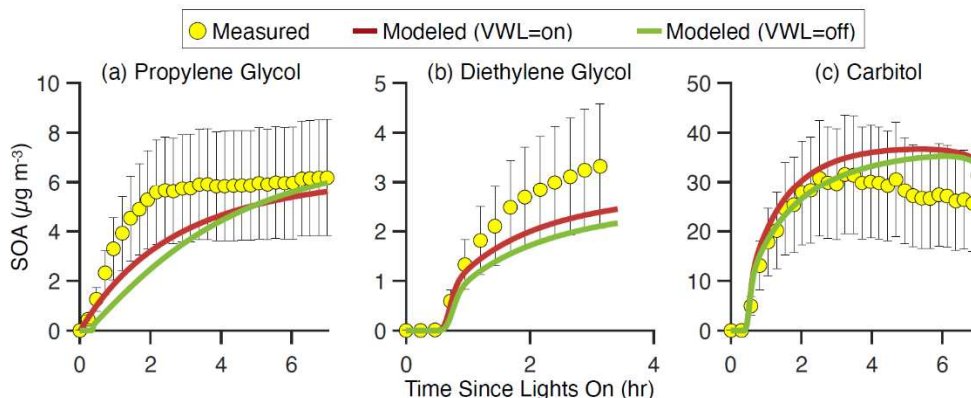


Figure 2: Predictions of SOA mass concentration from the SOM-TOMAS model compared to observations for three different OVOCs. These model-measurement comparison tests how well the parameters developed from a different experiment work for the shown experiments. Predictions are shown in solid lines (dull red for VWL=on and lime green for VWL=off) while observations are shown as symbols (yellow circles). SOA parameters (VWL=on and VWL=off) used with the SOM-TOMAS model for these OVOCs are listed in Table 2.

Model predictions of SOA mass concentrations were underestimated for propylene glycol and diethylene glycol but still within the reported uncertainty for the observations ( $\pm 38\%$ ). Model predictions of SOA mass concentrations were only slightly overestimated for carbitol compared to the observations. The use of VWL=on and VWL=off parameters resulted in similar model predictions. Overall, these comparisons suggested that while there was some experiment-to-experiment variability in the chamber experiments for the same OVOC, the SOM-TOMAS parameters were able to generally reproduce the SOA formation under a slightly different set of initial conditions (see Table 1 for experiments used to fit the parameters and Table S1 for experiments used to evaluate the parameters). It needs to be re-iterated here that, the discrepancies

that you see here, are due to the inherent experiment-to-experiment variability, and not due to the ineffectiveness of the parameters developed. This provides confidence for broader use of the SOM-TOMAS parameters developed in this work.

Observations of SOA O:C were not accounted for in the fitting procedure as experiment-specific O:C data were only available for four of the ten experiments and in three of the experiments the data were not corrected for SOA formed by the surrogate mixture. Nevertheless, we qualitatively compared the predicted SOA O:C from the end of the experiment to observations, noting that those observations were not necessarily from the same experiment used to determine the fits. For carbitol and benzyl alcohol, the model-predicted SOA O:C of 1.0 and 0.85 was consistent with the SOA O:C range measured for these OVOCs across two different experiments (0.6-1.2 for carbitol and 0.8-0.86 for benzyl alcohol). The model slightly under- and over-estimated the SOA O:C for butyl carbitol (0.76) and dimethyl glutarate (0.95) compared to the observations (0.98 for butyl carbitol and 0.72 for dimethyl glutarate) but the model predictions were within the reported uncertainty for observations of SOA O:C ( $\pm 28\%$ , as per Canagratna et al.<sup>56</sup>). The model significantly overestimated the SOA O:C for propylene glycol (1.99), DPGMEA (0.81), and Texanol (0.52) compared to the observations (0.55 for propylene glycol, 0.17 for DPGMEA, and 0.34 for Texanol). For propylene glycol and DPGMEA, the observed SOA O:C (0.55 and 0.17, respectively) was lower than the O:C for the primary OVOC (0.67 for propylene glycol and 0.44 for DPGMEA) suggesting that these OVOCs may be reacting and fragmenting in ways that our statistical approach is unable to capture. In addition to comparing the end-of-experiment values, we examined the modeled and observed trends in SOA O:C with the carbon number of the OVOC and these results are shown in Figure 3.

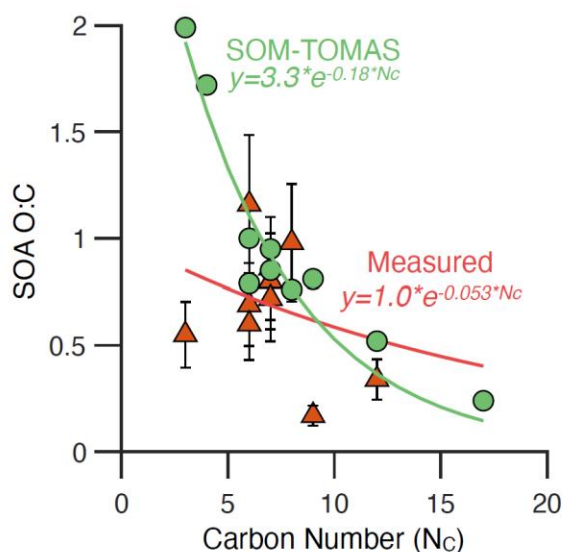


Figure 3: Modeled and observed SOA O:C ratios from the end of the experiment plotted against the carbon number of the OVOC (symbols). Solid lines are exponential fits to the data.

The red triangles in the figure denote the end-of-experiment measured O:C values segregated by the Carbon number, whereas the solid green circles are the SOM-TOMAS-predicted corresponding O:C results. The red & green lines are exponential fits to the measured & modeled data, respectively. Although there was some overlap between the modeled and observed SOA O:C values between OVOC carbon numbers of 6 and 8, they exhibited very different trends. The SOM-TOMAS-predicted SOA O:C understandably exhibited a stronger and tighter trend with carbon number but it was harder to see a similar trend in the observed values. To summarize, while the SOM-TOMAS predictions of O:C are roughly in the same range as the observations, the model-measurement comparison for SOA O:C is modest at best. It is likely that fitting SOM-TOMAS predictions to observations of SOA mass concentration and O:C simultaneously, as has been done in the past, would result in better constrained SOA parameters.

We explored the possibility of developing a unified set of SOM-TOMAS parameters for carbitol and butyl carbitol since the oxidation chemistry leading to SOA formation for these two

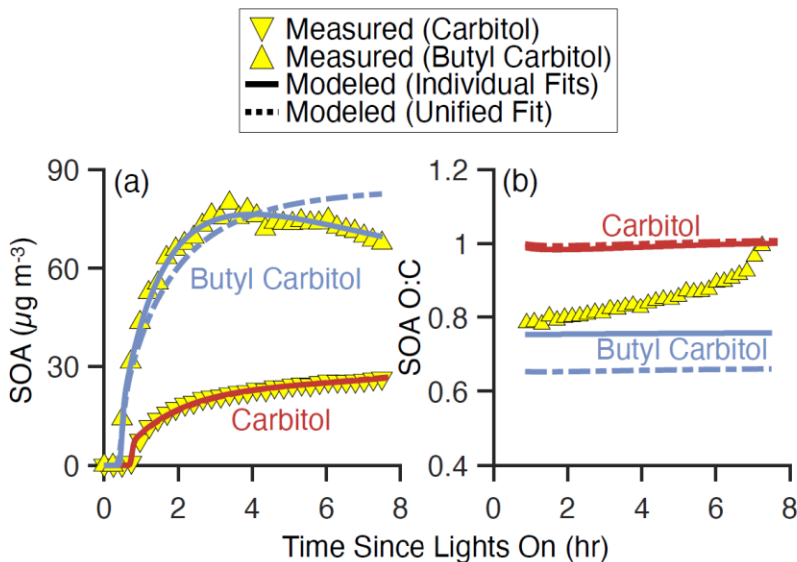


Figure 4: Predictions of (a) SOA mass concentration and (b) SOA O:C from the SOM-TOMAS model compared to chamber observations for high  $\text{NO}_x$  experiments performed with carbitol and butyl carbitol. Predictions from the individual fits are shown with solid lines, while those from the unified fit are shown with dashed lines. Observations are shown as symbols. There are no observations for SOA O:C for carbitol. SOA parameters (VWL=on) used with the SOM-TOMAS model are listed in Table 2.

OVOCs, who only differ from each other in the terminal alkyl group (ethyl versus butyl, respectively), might be similar. Results from performing separate fits are compared to those from performing unified fits in Figure 4.

Model predictions based on this unified parameter set reproduced observations of SOA mass concentration for both OVOCs with nearly the same level of fidelity as the separate sets. These fits, however, seemed to underpredict the O:C for Butyl Carbitol, compared to the standalone fits. Such universal parameter sets hold significant value in simulating the SOA formation from a lumped class of SOA precursors in CTMs.

### 3.2 SOA Parameterizations Based on Atmospheric Simulations

Output from the pseudo atmospheric simulations performed using the SOM-TOMAS model were used to develop two different kinds of parameterizations for VCP OVOCs: (i) a simple parameterization based on the carbon and oxygen numbers of the OVOC and (ii) VBS parameters for use in CTMs. The atmospheric simulations were based on the SOM-TOMAS parameters (VWL=on) listed in Table 2 for OVOCs and were based on SOM-TOMAS parameters from our previous work for hydrocarbons.<sup>31</sup> We should note that for both OVOCs and hydrocarbons, the

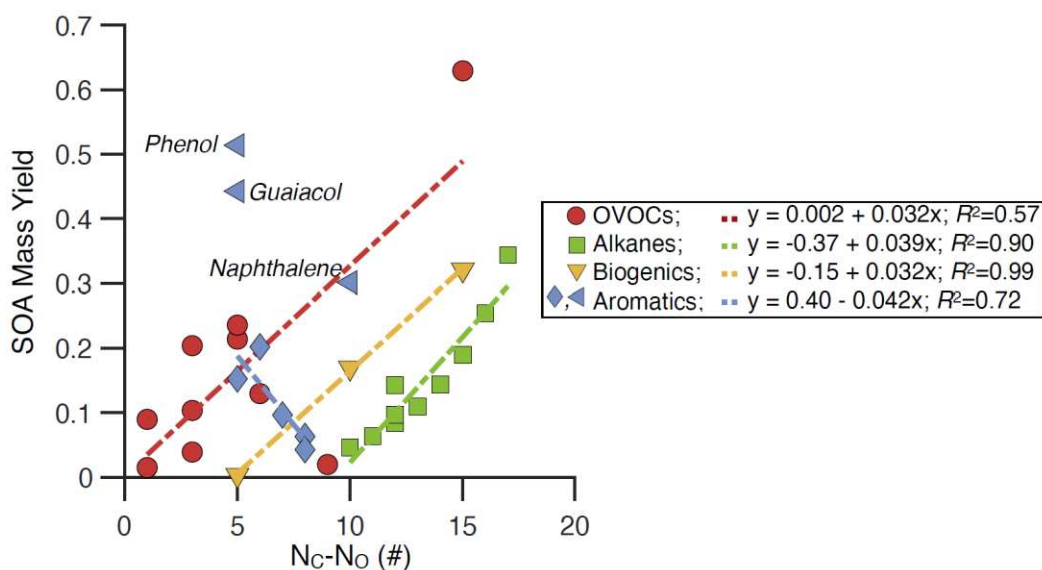


Figure 5: Predictions of SOA mass yields from atmospheric simulations (photochemical age=12 hours,  $OA=10 \mu\text{g m}^{-3}$ ) performed with the SOM-TOMAS model. Simulations for OVOCs were based on the parameters listed in Table 2 (VWL=on). Simulations for alkanes, biogenics, and aromatics were based on parameters developed in previous work.<sup>31</sup> Aromatic outliers (phenol, guaiacol, and naphthalene) are labeled explicitly and excluded from the linear fits.

parameters used to run these simulations were exclusively determined from environmental chamber data performed under high  $\text{NO}_x$  conditions.

In Figure 5, we plot the SOA mass yields from atmospheric simulations performed at an OA mass loading of  $10 \mu\text{g m}^{-3}$  and at a photochemical age of 12 hours against the quantity  $[N_C - N_O]$  (carbon number - oxygen number). The SOA mass yields, as we know, scale with Carbon

number, and have an inverse relationship with Oxygen number, owing to increased fragmentation. Hence, we subtract the Oxygen number, to account for the fragmentation effects. We found that the SOA mass yields for OVOCs exhibited a modest linear correlation with  $[N_C-N_O]$  ( $R^2=0.57$ ), with Texanol being an outlier (SOA mass yield of 0.02); the slope of the linear fit increased by 25% and the  $R^2$  changed to 0.88 if Texanol was removed from the fit. It is not clear as to why Texanol is an outlier, given that it is very vulnerable to fragmentation. This linear trend seemed intuitive since SOA production, as previously mentioned, has been shown to be proportional to the carbon number<sup>12,13,57</sup> and negatively affected by the presence of oxygen-containing functional groups (e.g., alcohol, carbonyl, acid),<sup>53,58,59</sup> for acyclic VOCs. The linear correlation was weakened when we considered different integer values for 'z' in  $[N_C-z \times N_O]$  ( $z=0, 1, 2, 3$ , etc.). When compared to the trends seen with OVOCs, the SOA mass yields for alkanes (based on parameters for *n*-dodecane, methylundecane, and hexylcyclohexane)<sup>60</sup> and biogenic VOCs (based on parameters for isoprene,  $\alpha$ -pinene, and  $\beta$ -caryophyllene)<sup>14,61</sup> showed a stronger correlation with  $[N_C]$  (since  $[N_C-N_O]=[N_C]$  for  $N_O=0$ );  $R^2=0.9$  for alkanes and  $R^2=0.99$  for biogenic VOCs. Furthermore, the trend lines for OVOCs, alkanes, and biogenic VOCs were nearly parallel to each other, offset by an  $[N_C-N_O]$  of  $\sim 4$ , suggesting that for the same  $[N_C-N_O]$  OVOCs take on higher SOA mass yields relative to biogenic OVOCs, followed by alkanes. The SOA mass yields for single-ring aromatics (based on parameters for benzene, toluene, *m*-xylene, *o*-xylene, phenol, guaiacol, syringol, and naphthalene)<sup>16,62-64</sup> did not show clear trends with  $[N_C-N_O]$ . If phenol, guaiacol, and naphthalene were treated as outliers (no specific reason), the SOA mass yields for single-ring aromatics exhibited a negative correlation with  $[N_C-N_O]$  ( $R^2=0.72$ ). Interestingly, the SOA mass yield for benzyl alcohol (0.13) with an  $[N_C-N_O]$  of 6 was in between that for syringol (SOA mass yield of 0.15 and with an  $[N_C-N_O]$  of 5) and toluene (SOA mass yield of 0.096 and

with an  $[N_C-N_O]$  of 7). The SOA mass yield trends shown for hydrocarbons are for illustrative purposes and to facilitate comparisons with those for OVOCs.

Overall, we found that the SOA mass yields for OVOCs were on the same order of magnitude or higher (after correcting for the presence of oxygen-containing functional groups) as previously well-studied VOCs. It is important to note that the SOA parameterization for OVOCs, presented here (i.e.,  $y=0.002+0.032\times[N_C-N_O]$ ), is based on a limited set of environmental chamber data. Accordingly, we advise that this parameterization only be used in the absence of experimental data or when a rough estimate is needed for the SOA mass yield for a new OVOC, representative of conditions in a typical urban environment.

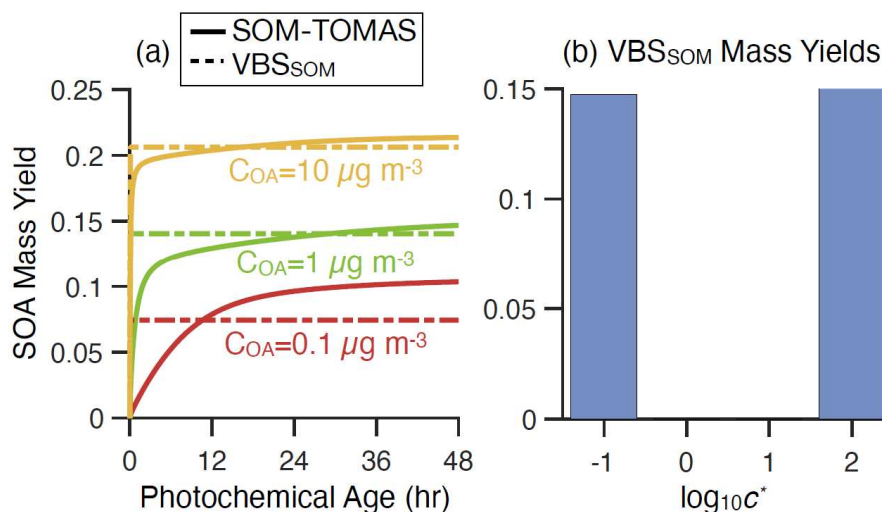


Figure 6: (a) Predictions from the SOM-TOMAS and VBS<sub>SOM</sub> models for the pseudo atmospheric simulations for carbitol at three different OA mass concentrations. Predictions from the VBS<sub>SOM</sub> model are based on VBS fits to the SOM-TOMAS model results. The VBS fits are listed for carbitol (along with other OVOCs) in Table 2. (b) VBS fits presented for carbitol as a function of  $c^*$ .

The time-varying SOA mass yields from the atmospheric simulations at three different OA mass loadings were used to fit VBS<sub>SOM</sub> parameters for use in CTMs. Results for carbitol, as a

representative choice, are shown in Figure 6. An instantaneous partitioning model based on the  $VBS_{SOM}$  parameters was able to generally reproduce the OA mass concentration-dependent SOA mass yield at photochemical ages longer than 12 hours but it overestimated the SOA mass yield at shorter times (Figure 6a). As mentioned in Section 2.3, this was because we deliberately chose to fit a static set of products that did not react further, which resulted in a fixed mass yield with time. Results for all OVOCs are shown in Figure S2 and  $VBS_{SOM}$  parameters for all OVOCs are listed in Table 3.

*Table 3: VBS parameters based on fitting the SOM-TOMAS model output from pseudo atmospheric simulations at three COA values: 0.1, 1, and 10  $\mu\text{g m}^{-3}$ . The SOM-TOMAS parameters used in these simulations are from Table 2 (VWL=on).*

VCP OVOC	$\log_{10}c^*$			
	0.1	1	10	100
Propylene Glycol	0.0919	0.0000	0.0000	0.0000
Diethylene Glycol	0.0149	0.0000	0.0000	0.0017
Carbitol	0.1473	0.0000	0.0000	0.6652
Triethanolamine	0.0221	0.0159	0.1008	0.1618
Benzyl Alcohol	0.0000	0.1513	0.1592	0.0001
Dimethyl Glutarate	0.0051	0.0020	0.0507	0.0684
Butyl Carbitol	0.0000	0.0100	0.3734	0.0166
DPGMEA	0.2326	0.0000	0.0000	0.2138
Texanol	0.0009	0.0145	0.0088	0.0046
Methyl Palmitate	0.6572	0.0000	0.0000	0.0000

In general, results for these other OVOCs were similar to those shown in Figure 6 for carbitol, with one exception (i.e., benzyl alcohol). Characteristic SOA mass yield versus OA mass concentration curves based on the  $VBS_{SOM}$  parameters for all ten OVOCs are shown in Figure 7. These curves are useful in visualizing the rank order for OVOCs for their potential to form SOA as well as quantifying the SOA mass yields at different OA mass loadings.

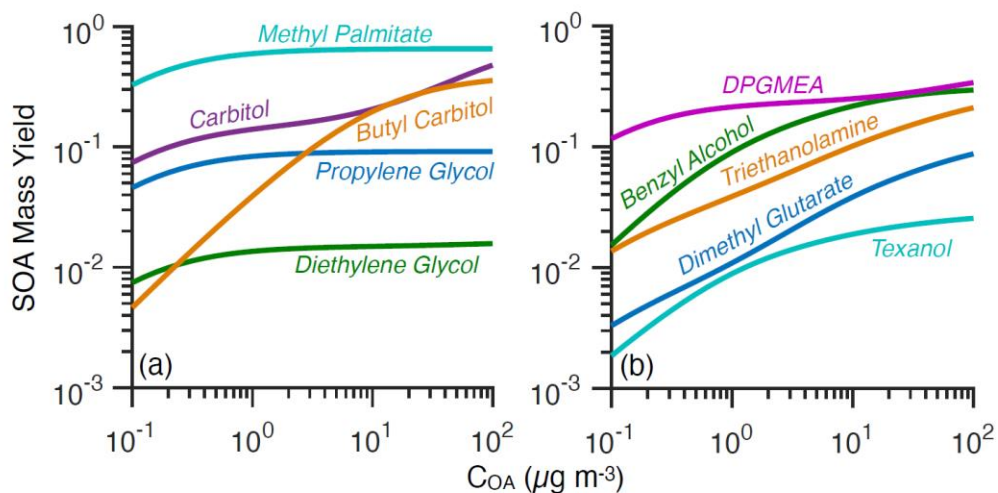


Figure 7: SOA mass yields plotted against OA mass concentrations based on the  $VBS_{SOM}$  parameters determined from atmospheric simulations performed with SOM-TOMAS. The yield curves are split across two panels (a and b) for visual clarity.

The  $VBS_{SOM}$  parameters listed in Table 3 are for individual OVOCs and do not provide direct guidance on how these need to be implemented in CTMs aiming to simulate the SOA contribution from VCP sources. For propylene glycol, we recommend treating that it as an explicit species in chemical mechanisms due to its implications for PAN formation combined with significant emissions and potential to form SOA.<sup>6</sup> In addition, we propose the following surrogate schemes based on a qualitative interpretation of the yield-loading curves presented in Figure 7. For a lower bound estimate of SOA, we propose using the  $VBS_{SOM}$  parameters for diethylene glycol for all glycols, butyl carbitol for all glycol ethers, and Texanol for all esters and acetates. For an upper bound estimate of SOA, we propose using the  $VBS_{SOM}$  parameters for propylene glycol for all glycols, carbitol for all glycol ethers, and DPGMEA for all esters and acetates. Oxygenated aromatics could be represented using the  $VBS_{SOM}$  parameters for benzyl alcohol. These surrogate assignments do not aim to cover the entire diversity of VCP OVOCs and more work is needed to help target OVOCs for future experimentation with chambers and flow reactors.

#### 4. Implications for Anthropogenic SOA

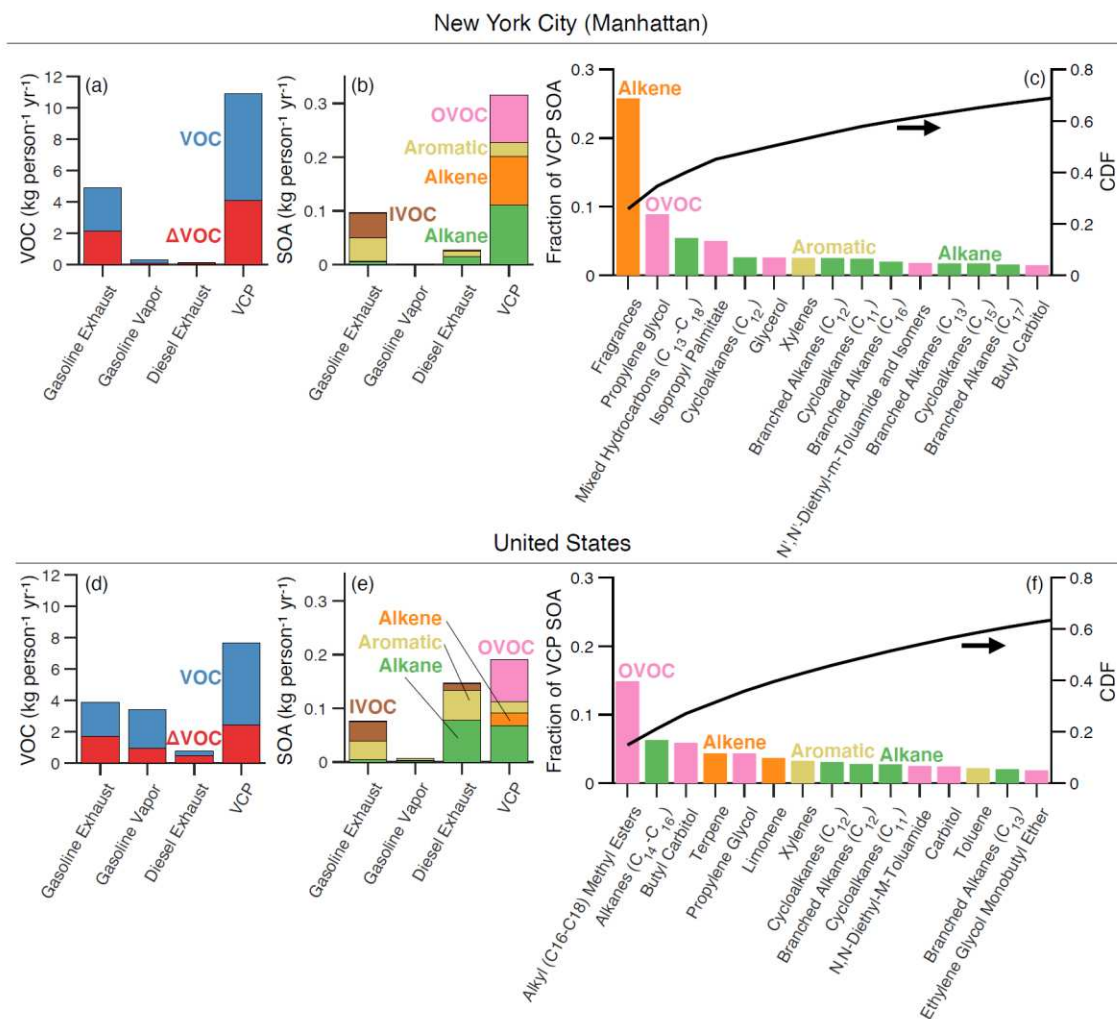


Figure 8: (a,d) VOC (blue bars) and reacted VOC ( $\Delta$ VOC) (red bars) and (b,e) SOA estimates from mobile sources and VCP use in (a,b,c) NYC and (d,e,f) the US. VOC and SOA estimates are calculated for a photochemical age of 12 hours and an OA mass loading of  $10 \mu\text{g m}^{-3}$ , representative of high  $\text{NO}_x$  conditions. SOA is resolved by precursor class. (c,f) Fractional contribution of VOCs to VCP-related SOA for the top fifteen species.

VOC emissions from mobile sources and VCP use were combined with SOA mass yields from the SOM-TOMAS atmospheric simulations to estimate SOA production resolved by source and precursor class. Results for NYC are shown in Figure 8. VOC emissions from VCP use ( $10.9 \text{ kg person}^{-1} \text{ yr}^{-1}$ ) were more than twice that from gasoline exhaust ( $4.9 \text{ kg person}^{-1} \text{ yr}^{-1}$ ), which constituted most of the emissions from mobile sources (i.e., on- and off-road gasoline, evaporated

gasoline vapors, and on- and off-road diesel) in NYC. After 12 hours of photochemical aging, a comparable amount of VOCs from VCP use had reacted (37%) compared to those from mobile sources (43%). With more emissions and a higher OH reactivity, VCP use resulted in much stronger (2.5×) SOA production ( $0.32 \text{ kg person}^{-1} \text{ yr}^{-1}$ ) compared to mobile sources ( $0.12 \text{ kg person}^{-1} \text{ yr}^{-1}$ ). Amongst VCP VOCs, hydrocarbons (i.e., alkanes, alkenes, and aromatics) accounted for most of the VCP-related SOA, with OVOCs contributing to 28% of the SOA. An examination of the top fifteen VOCs that were responsible for more than two-thirds of the VCP SOA offered a few additional insights: (i) fragrances that are primarily composed of terpenes and terpenoids<sup>65</sup> accounted for a quarter of all VCP-related SOA, (ii) many of the important VCP SOA precursors were long-chain ( $\text{C}_{10+}$ ) branched and cyclic alkanes, and (iii) glycols (propylene glycol, glycerol) and a single methyl ester (isopropyl palmitate), insect repellent (N,N-Diethyl-m-toluamide), and glycol ether (carbitol) were amongst the top OVOCs contributing to VCP SOA. Results for SoCAB are shown in Figure S3 and, despite the use of a coarser emissions inventory, the findings were generally consistent with those presented for NYC (Section S2).

Coming to the fraction of VOCs emitted indoors that make it outside, it can depend on a host of factors such as the compound being emitted, indoor oxidant levels, geographical location, & physical conditions. As an example, the indoor emissions react with oxidants such as  $\text{O}_3$  among others. So, in the limit of zero chemical losses, the indoor emissions will equal the emissions to the ambient air. For molecules reactive with  $\text{O}_3$  in indoor air, such as Terpenes, chemical losses indoors will decrease the amount that is transported outside. Under typical ambient levels of  $\text{O}_3$  (50-80 ppb) observed across the LA basin during the 2010 CalNex study, 5-30% of terpenes emitted indoors can react from ozonolysis.<sup>1</sup> So, it would be fair to say that 70-95% of the terpenes emitted indoors are transported outdoors.

Results for the US, which uses a separate emissions estimation approach, are also shown in Figure 8 and these appeared to be slightly different from those presented for SoCAB and NYC. VOC emissions from VCP use ( $7.6 \text{ kg person}^{-1} \text{ yr}^{-1}$ ) were slightly lower than those from mobile sources ( $8 \text{ kg person}^{-1} \text{ yr}^{-1}$ ) and, hence, SOA production was proportionately lower ( $0.19$  versus  $0.23 \text{ kg person}^{-1} \text{ yr}^{-1}$ , respectively). Despite those differences, some of the same precursor categories (e.g., alkanes, OVOCs) and classes (e.g., branched and cyclic alkanes, terpenes, glycols, glycol ethers, esters, insect repellents) were found to contribute the most to VCP SOA. The top fifteen VOCs accounted for slightly less than two-thirds of the total VCP SOA. There were three key differences between the US and NYC/SoCAB results. First, large alkyl methyl esters were the dominant species contributing to VCP SOA nationally ( $15\%$  of the total) while fragrances were the dominant species in NYC/SoCAB. Second, OVOCs accounted for more than  $40\%$  of the VCP SOA nationally but  $\sim 27\%$  of the VCP SOA in NYC/SoCAB. Third, diesel (on- and non-road) sources contributed more to SOA than gasoline sources in the US, highlighting the larger proportion of diesel to gasoline sources nationally, relative to NYC and SoCAB. A compilation of the top 50 VOCs contributing to VCP SOA for all three regions is provided in Tables S5 through S7. One key takeaway from this analysis that would be of particular significance to EPA is that, to cut down on the SOA formation from VCP sources, one should probably focus on reformulating the products with non-oxygenated VOC species with lower SOA forming potentials. The OVOC species may be overlooked, considering their relatively low SOA contributions.

The results described above were calculated for photochemical ages of 12 hours and a background OA mass loading of  $10 \mu\text{g m}^{-3}$  to keep the findings relevant for cities. To investigate

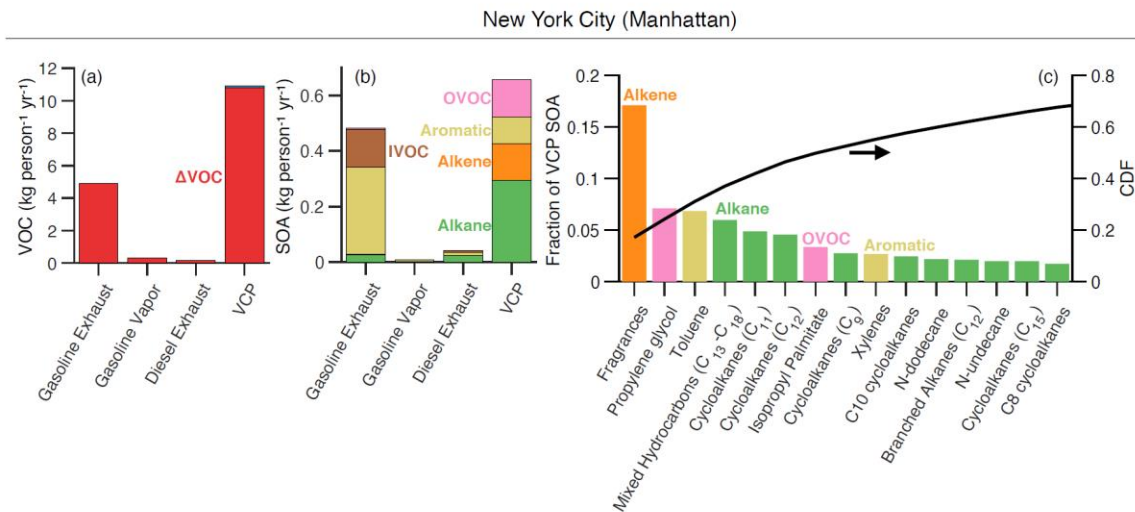


Figure 9: Same as Figure 8(a,b,c) but with all VOC reacted.

the maximum potential to form SOA, we performed the same analysis for the NYC emissions assuming all SOA precursors had completely reacted and those results are presented in Figure 9.

Here, the VCP SOA was only 1.2 $\times$  the mobile source SOA, a much smaller difference compared to the 2.5 $\times$  difference found at the city-relevant photochemical age. This was largely because the important SOA precursors in gasoline exhaust are single-ring aromatics and IVOCs, both of which reacted much more slowly than the more reactive VOCs found in VCP emissions. As shown in Figure 9, SOA production from VCP use only doubled (from 0.32 to 0.66  $\text{kg person}^{-1} \text{yr}^{-1}$ ) while SOA production from mobile sources more than quadrupled (from 0.12 to 0.53  $\text{kg person}^{-1} \text{yr}^{-1}$ ).

If results from the calculations above can be extrapolated for the US population, VCP use would contribute to 60 to 130  $\text{Gg yr}^{-1}$  of SOA 12 hours after emission and a maximum of 160 to 310  $\text{Gg yr}^{-1}$  of SOA (ignoring that at regional/global scales the OA mass loading and  $\text{NO}_x$  levels

would be much lower and other atmospheric processes might be more important (e.g., deposition, photolysis)). The VCP contributions to anthropogenic SOA and PM<sub>2.5</sub> are significant since mobile sources, as a widely regulated source of air pollutants, are estimated to contribute to PM<sub>2.5</sub> on a similar scale: 100 Gg yr<sup>-1</sup> of primary OA and a maximum of 200 Gg yr<sup>-1</sup> of SOA.<sup>66</sup> Quantifying the magnitude and the composition of atmospheric VCP VOC emissions is an active area of research and, hence, the calculations performed in this work and the comparisons made with mobile source SOA need to be interpreted with care.

## REFERENCES

- (1) McDonald, B. C.; de Gouw, J. A.; Gilman, J. B.; Jathar, S. H.; Akherati, A.; Cappa, C. D.; Jimenez, J. L.; Lee-Taylor, J.; Hayes, P. L.; McKeen, S. A.; Cui, Y. Y.; Kim, S.-W.; Gentner, D. R.; Isaacman-VanWertz, G.; Goldstein, A. H.; Harley, R. A.; Frost, G. J.; Roberts, J. M.; Ryerson, T. B.; Trainer, M. Volatile Chemical Products Emerging as Largest Petrochemical Source of Urban Organic Emissions. *Science* **2018**, *359* (6377), 760–764.
- (2) Karl, T.; Striednig, M.; Graus, M.; Hammerle, A.; Wohlfahrt, G. Urban Flux Measurements Reveal a Large Pool of Oxygenated Volatile Organic Compound Emissions. *Proceedings of the National Academy of Sciences* **2018**, *115* (6), 1186–1191.
- (3) Francoeur, C. B.; McDonald, B. C.; Gilman, J. B.; Zarzana, K. J.; Dix, B.; Brown, S. S.; de Gouw, J. A.; Frost, G. J.; Li, M.; McKeen, S. A.; Peischl, J.; Pollack, I. B.; Ryerson, T. B.; Thompson, C.; Warneke, C.; Trainer, M. Quantifying Methane and Ozone Precursor Emissions from Oil and Gas Production Regions across the Contiguous US. *Environ. Sci. Technol.* **2021**, *55* (13), 9129–9139.
- (4) Qin, M.; Murphy, B. N.; Isaacs, K. K.; McDonald, B. C.; Lu, Q.; McKeen, S. A.; Koval, L.; Robinson, A. L.; Efstathiou, C.; Allen, C.; Pye, H. O. T. Criteria Pollutant Impacts of Volatile Chemical Products Informed by near-Field Modeling. *Nat Sustain* **2020**, *N/A*, 1–57.
- (5) Gkatzelis, G. I.; Coggon, M. M.; McDonald, B. C.; Peischl, J.; Aikin, K. C.; Gilman, J. B.; Trainer, M.; Warneke, C. Identifying Volatile Chemical Product Tracer Compounds in U.S. Cities. *Environ. Sci. Technol.* **2021**, *55* (1), 188–199.
- (6) Coggon, M. M.; Gkatzelis, G. I.; McDonald, B. C.; Gilman, J. B.; Schwantes, R. H.; Abuhassan, N.; Aikin, K. C.; Arend, M. F.; Berkoff, T. A.; Brown, S. S.; Campos, T. L.; Dickerson, R. R.; Gronoff, G.; Hurley, J. F.; Isaacman-VanWertz, G.; Koss, A. R.; Li, M.; McKeen, S. A.; Moshary, F.; Peischl, J.; Pospisilova, V.; Ren, X.; Wilson, A.; Wu, Y.; Trainer, M.; Warneke, C. Volatile Chemical Product Emissions Enhance Ozone and Modulate Urban Chemistry. *Proc. Natl. Acad. Sci. U. S. A.* **2021**, *118* (32). <https://doi.org/10.1073/pnas.2026653118>.
- (7) Gkatzelis, G. I.; Coggon, M. M.; McDonald, B. C.; Peischl, J.; Gilman, J. B.; Aikin, K. C.; Robinson, M. A.; Canonaco, F.; Prevot, A. S. H.; Trainer, M.; Warneke, C. Observations Confirm That Volatile Chemical Products Are a Major Source of Petrochemical Emissions in U.S. Cities. *Environ. Sci. Technol.* **2021**, *55* (8), 4332–4343.
- (8) Khare, P.; Krechmer, J. E.; Machesky, J. E.; Hass-Mitchell, T.; Cao, C.; Wang, J.; Majluf, F.; Lopez-Hilfiker, F.; Malek, S.; Wang, W.; Seltzer, K.; Pye, H. O. T.; Commane, R.; McDonald, B. C.; Toledo-Crow, R.; Mak, J. E.; Gentner, D. R. Ammonium-Adduct Chemical Ionization to Investigate Anthropogenic Oxygenated Gas-Phase Organic Compounds in Urban Air, 2022. <https://doi.org/10.5194/acp-2022-421>.
- (9) Pennington, E. A.; Seltzer, K. M.; Murphy, B. N.; Qin, M.; Seinfeld, J. H.; Pye, H. O. T. Modeling Secondary Organic Aerosol Formation from Volatile Chemical Products. *Atmos. Chem. Phys.* **2021**, *21* (24), 18247–18261.
- (10) Seltzer, K. M.; Murphy, B. N.; Pennington, E. A.; Allen, C.; Talgo, K.; Pye, H. O. T. Volatile Chemical Product Enhancements to Criteria Pollutants in the United States. *Environ. Sci. Technol.* **2022**, *56* (11), 6905–6913.
- (11) Seltzer, K. M.; Pennington, E.; Rao, V.; Murphy, B. N.; Strum, M.; Isaacs, K. K.; Pye, H. O. T. Reactive Organic Carbon Emissions from Volatile Chemical Products. *Atmos. Chem. Phys.* **2021**, *21* (6), 5079–5100.
- (12) Lim, Y. B.; Ziemann, P. J. Effects of Molecular Structure on Aerosol Yields from OH Radical-Initiated Reactions of Linear, Branched, and Cyclic Alkanes in the Presence of NO<sub>x</sub>. *Environ. Sci. Technol.* **2009**, *43* (7), 2328–2334.
- (13) Presto, A. A.; Miracolo, M. A.; Donahue, N. M.; Robinson, A. L. Secondary Organic Aerosol

- Formation from High-NO(x) Photo-Oxidation of Low Volatility Precursors: N-Alkanes. *Environ. Sci. Technol.* **2010**, *44* (6), 2029–2034.
- (14) Ng, N. L.; Kroll, J. H.; Keywood, M. D.; Bahreini, R.; Varutbangkul, V.; Flagan, R. C.; Seinfeld, J. H.; Lee, A.; Goldstein, A. H. Contribution of First- versus Second-Generation Products to Secondary Organic Aerosols Formed in the Oxidation of Biogenic Hydrocarbons. *Environ. Sci. Technol.* **2006**, *40* (7), 2283–2297.
- (15) Paulot, F.; Crouse, J. D.; Kjaergaard, H. G.; Kroll, J. H.; Seinfeld, J. H.; Wennberg, P. O. Isoprene Photooxidation: New Insights into the Production of Acids and Organic Nitrates. *Atmos. Chem. Phys.* **2009**, *9* (4), 1479–1501.
- (16) Ng, N. L.; Chhabra, P. S.; Chan, A. W. H.; Surratt, J. D.; Kroll, J. H.; Kwan, A. J.; McCabe, D. C.; Wennberg, P. O.; Sorooshian, A.; Murphy, S. M.; Dalleska, N. F.; Flagan, R. C.; Seinfeld, J. H. Effect of NO<sub>x</sub> Level on Secondary Organic Aerosol (SOA) Formation from the Photooxidation of Terpenes. *Atmospheric Chemistry and Physics*. 2007, pp 5159–5174. <https://doi.org/10.5194/acp-7-5159-2007>.
- (17) Li, L.; Tang, P.; Nakao, S.; Cocker, D. R., III. Impact of Molecular Structure on Secondary Organic Aerosol Formation from Aromatic Hydrocarbon Photooxidation under Low-NO<sub>x</sub> Conditions. *Atmos. Chem. Phys.* **2016**, *16* (17), 10793–10808.
- (18) Li, W.; Li, L.; Chen, C.-L.; Kacarab, M.; Peng, W.; Price, D.; Xu, J.; Cocker, D. R. Potential of Select Intermediate-Volatility Organic Compounds and Consumer Products for Secondary Organic Aerosol and Ozone Formation under Relevant Urban Conditions. *Atmos. Environ.* **2018**, *178*, 109–117.
- (19) Charan, S. M.; Buenconsejo, R. S.; Seinfeld, J. H. Secondary Organic Aerosol Yields from the Oxidation of Benzyl Alcohol. *Atmos. Chem. Phys.* **2020**, *20* (21), 13167–13190.
- (20) Humes, M. B.; Wang, M.; Kim, S.; Machesky, J. E.; Gentner, D. R.; Robinson, A. L.; Donahue, N. M.; Presto, A. A. Limited Secondary Organic Aerosol Production from Acyclic Oxygenated Volatile Chemical Products. *Environ. Sci. Technol.* **2022**, *56* (8), 4806–4815.
- (21) Lu, Q.; Murphy, B. N.; Qin, M.; Adams, P. J.; Zhao, Y.; Pye, H. O. T.; Efstathiou, C.; Allen, C.; Robinson, A. L. Simulation of Organic Aerosol Formation during the CalNex Study: Updated Mobile Emissions and Secondary Organic Aerosol Parameterization for Intermediate-Volatility Organic Compounds. *Atmos. Chem. Phys.* **2020**, *20* (7), 4313–4332.
- (22) Wu, Y.; Johnston, M. V. Aerosol Formation from OH Oxidation of the Volatile Cyclic Methyl Siloxane (cVMS) Decamethylcyclopentasiloxane. *Environ. Sci. Technol.* **2017**, *51* (8), 4445–4451.
- (23) Li, L.; Cocker, D. R. Molecular Structure Impacts on Secondary Organic Aerosol Formation from Glycol Ethers. *Atmos. Environ.* **2018**, *180*, 206–215.
- (24) Janecek, N. J.; Marek, R. F.; Bryngelson, N.; Singh, A.; Bullard, R. L.; Brune, W. H.; Stanier, C. O. Physical Properties of Secondary Photochemical Aerosol from OH Oxidation of a Cyclic Siloxane. *Atmos. Chem. Phys.* **2019**, *19* (3), 1649–1664.
- (25) Han, S.; Jang, M. Modeling Diurnal Variation of SOA Formation via Multiphase Reactions of Biogenic Hydrocarbons, 2022. <https://doi.org/10.5194/acp-2022-327>.
- (26) Charan, S. M.; Huang, Y.; Buenconsejo, R. S. Secondary Organic Aerosol Formation from the Oxidation of Decamethylcyclopentasiloxane at Atmospherically Relevant OH Concentrations. *Atmospheric* **2022**.
- (27) Cocker, D. R., 3rd; Flagan, R. C.; Seinfeld, J. H. State-of-the-Art Chamber Facility for Studying Atmospheric Aerosol Chemistry. *Environ. Sci. Technol.* **2001**, *35* (12), 2594–2601.
- (28) Carter, W. P. L.; Cocker, D. R., III; Fitz, D. R.; Malkina, I. L. A New Environmental Chamber for Evaluation of Gas-Phase Chemical Mechanisms and Secondary Aerosol Formation. *Atmospheric* **2005**.
- (29) Cappa, C. D.; Wilson, K. R. Multi-Generation Gas-Phase Oxidation, Equilibrium Partitioning, and the Formation and Evolution of Secondary Organic Aerosol. *Atmos. Chem. Phys.* **2012**, *12* (20), 9505–9528.
- (30) Adams, P.; Seinfeld, J. Predicting Global Aerosol Size Distributions in General Circulation Models. *Journal of Geophysical Research Atmospheres* **2002**. <https://doi.org/10.1029/2001JD001010>.
- (31) Akherati, A.; He, Y.; Coggon, M. M.; Koss, A. R.; Hodshire, A. L.; Sekimoto, K.; Warneke, C.; de Gouw, J.; Yee, L.; Seinfeld, J. H.; Onasch, T. B.; Herndon, S. C.; Knighton, W. B.; Cappa, C. D.;

- Kleeman, M. J.; Lim, C. Y.; Kroll, J. H.; Pierce, J. R.; Jathar, S. H. Oxygenated Aromatic Compounds Are Important Precursors of Secondary Organic Aerosol in Biomass-Burning Emissions. *Environ. Sci. Technol.* **2020**, *54* (14), 8568–8579.
- (32) He, Y.; Lambe, A. T.; Seinfeld, J. H.; Cappa, C. D.; Pierce, J. R.; Jathar, S. H. Process-Level Modeling Can Simultaneously Explain Secondary Organic Aerosol Evolution in Chambers and Flow Reactors. *Environ. Sci. Technol.* **2022**, *56* (10), 6262–6273.
- (33) He, Y.; King, B.; Pothier, M.; Lewane, L.; Akherati, A.; Mattila, J.; Farmer, D. K.; McCormick, R. L.; Thornton, M.; Pierce, J. R.; Volckens, J.; Jathar, S. H. Secondary Organic Aerosol Formation from Evaporated Biofuels: Comparison to Gasoline and Correction for Vapor Wall Losses. *Environ. Sci. Process. Impacts* **2020**, *22* (7), 1461–1474.
- (34) Akherati, A.; He, Y.; Garofalo, L. A.; Hodshire, A. L.; Farmer, D. K.; Kreidenweis, S. M.; Permar, W.; Hu, L.; Fischer, E. V.; Jen, C. N.; Goldstein, A. H.; Levin, E. J. T.; DeMott, P. J.; Campos, T. L.; Flocke, F.; Reeves, J. M.; Toohey, D. W.; Pierce, J. R.; Jathar, S. H. Dilution and Photooxidation Driven Processes Explain the Evolution of Organic Aerosol in Wildfire Plumes. *Environ. Sci.: Atmos.* **2022**, *2* (5), 1000–1022.
- (35) Zaveri, R. A.; Easter, R. C.; Shilling, J. E. Modeling Kinetic Partitioning of Secondary Organic Aerosol and Size Distribution Dynamics: Representing Effects of Volatility, Phase State, and Particle-Phase Reaction. *Chemistry and Physics* **2014**.
- (36) Matsunaga, A.; Ziemann, P. J. Gas-Wall Partitioning of Organic Compounds in a Teflon Film Chamber and Potential Effects on Reaction Product and Aerosol Yield Measurements. *Aerosol Science and Technology* **2010**. <https://doi.org/10.1080/02786826.2010.501044>.
- (37) Krechmer, J. E.; Pagonis, D.; Ziemann, P. J.; Jimenez, J. L. Quantification of Gas-Wall Partitioning in Teflon Environmental Chambers Using Rapid Bursts of Low-Volatility Oxidized Species Generated in Situ. *Environ. Sci. Technol.* **2016**, *50* (11), 5757–5765.
- (38) Zhang, X.; Cappa, C. D.; Jathar, S. H.; McVay, R. C.; Ensberg, J. J.; Kleeman, M. J.; Seinfeld, J. H. Influence of Vapor Wall Loss in Laboratory Chambers on Yields of Secondary Organic Aerosol. *Proc. Natl. Acad. Sci. U. S. A.* **2014**, *111* (16), 5802–5807.
- (39) Ehn, M.; Thornton, J. A.; Kleist, E.; Sipilä, M.; Junninen, H.; Pullinen, I.; Springer, M.; Rubach, F.; Tillmann, R.; Lee, B.; Lopez-Hilfiker, F.; Andres, S.; Acir, I.-H.; Rissanen, M.; Jokinen, T.; Schobesberger, S.; Kangasluoma, J.; Kontkanen, J.; Nieminen, T.; Kurtén, T.; Nielsen, L. B.; Jørgensen, S.; Kjaergaard, H. G.; Canagaratna, M.; Maso, M. D.; Berndt, T.; Petäjä, T.; Wahner, A.; Kerminen, V.-M.; Kulmala, M.; Worsnop, D. R.; Wildt, J.; Mentel, T. F. A Large Source of Low-Volatility Secondary Organic Aerosol. *Nature* **2014**, *506* (7489), 476–479.
- (40) Shiraiwa, M.; Zuend, A.; Bertram, A. K. Gas–particle Partitioning of Atmospheric Aerosols: Interplay of Physical State, Non-Ideal Mixing and Morphology. *Annu. Rep. Prog. Chem. Sect. C: Phys. Chem.* **2013**.
- (41) D’Ambro, E. L.; Schobesberger, S.; Zaveri, R. A.; Shilling, J. E.; Lee, B. H.; Lopez-Hilfiker, F. D.; Mohr, C.; Thornton, J. A. Isothermal Evaporation of  $\alpha$ -Pinene Ozonolysis SOA: Volatility, Phase State, and Oligomeric Composition. *ACS Earth Space Chem.* **2018**, *2* (10), 1058–1067.
- (42) Bahreini, R.; Ervens, B.; Middlebrook, A. M.; Warneke, C.; de Gouw, J. A.; DeCarlo, P. F.; Jimenez, J. L.; Brock, C. A.; Neuman, J. A.; Ryerson, T. B.; Stark, H.; E. Atlas; Brioude, J.; Fried, A.; Holloway, J. S.; Peischl, J.; Richter, D.; Walega, J.; Weibring, P.; Wollny, A. G.; Fehsenfeld, F. C. Organic Aerosol Formation in Urban and Industrial Plumes near Houston and Dallas, Texas. *J. Geophys. Res.* **2009**, *114* (D00F16). <https://doi.org/10.1029/2008jd011493>.
- (43) Bilsback, K.; He, Y.; Cappa, C.; Chan, A.; Pierce, J.; Ng, N. L.; Seinfeld, J.; Jathar, S. Vapors Are Lost to Walls, Not to Particles on the Wall: Development of Artifact-Corrected Parameters and Implications for Global Secondary Organic Aerosol; 2021; Vol. 2021, p A23D – 03.
- (44) Porter, W. C.; Jimenez, J. L.; Barsanti, K. C. Quantifying Atmospheric Parameter Ranges for Ambient Secondary Organic Aerosol Formation. *ACS Earth Space Chem.* **2021**, *5* (9), 2380–2397.
- (45) Shrivastava, M.; Andreae, M. O.; Artaxo, P.; Barbosa, H. M. J.; Berg, L. K.; Brito, J.; Ching, J.; Easter, R. C.; Fan, J.; Fast, J. D.; Feng, Z.; Fuentes, J. D.; Glasius, M.; Goldstein, A. H.; Alves, E. G.;

- Gomes, H.; Gu, D.; Guenther, A.; Jathar, S. H.; Kim, S.; Liu, Y.; Lou, S.; Martin, S. T.; McNeill, V. F.; Medeiros, A.; de Sá, S. S.; Shilling, J. E.; Springston, S. R.; Souza, R. A. F.; Thornton, J. A.; Isaacman-VanWertz, G.; Yee, L. D.; Ynoue, R.; Zaveri, R. A.; Zelenyuk, A.; Zhao, C. Urban Pollution Greatly Enhances Formation of Natural Aerosols over the Amazon Rainforest. *Nat. Commun.* **2019**, *10* (1), 1046.
- (46) Pai, S. J.; Heald, C. L.; Pierce, J. R.; Farina, S. C.; Marais, E. A.; Jimenez, J. L.; Campuzano-Jost, P.; Nault, B. A.; Middlebrook, A. M.; Coe, H.; Shilling, J. E.; Bahreini, R.; Dingle, J. H.; Vu, K. An Evaluation of Global Organic Aerosol Schemes Using Airborne Observations. *Atmos. Chem. Phys.* **2020**. <https://doi.org/10.5194/acp-20-2637-2020>.
- (47) McDonald, B. C.; McKeen, S. A.; Cui, Y. Y.; Ahmadov, R.; Kim, S.-W.; Frost, G. J.; Pollack, I. B.; Peischl, J.; Ryerson, T. B.; Holloway, J. S.; Graus, M.; Warneke, C.; Gilman, J. B.; de Gouw, J. A.; Kaiser, J.; Keutsch, F. N.; Hanisco, T. F.; Wolfe, G. M.; Trainer, M. Modeling Ozone in the Eastern U.S. Using a Fuel-Based Mobile Source Emissions Inventory. *Environ. Sci. Technol.* **2018**, *52* (13), 7360–7370.
- (48) EPA. 2017 National Emissions Inventory (NEI) Data, 2021.
- (49) Atkinson, R.; Arey, J. Atmospheric Degradation of Volatile Organic Compounds. *Chem. Rev.* **2003**, *103* (12), 4605–4638.
- (50) Hayes, P. L.; Carlton, A. G.; Baker, K. R.; Ahmadov, R.; Washenfelder, R. A.; Alvarez, S.; Rappenglück, B.; Gilman, J. B.; Kuster, W. C.; de Gouw, J. A.; Zotter, P.; Prévôt, A. S. H.; Szidat, S.; Kleindienst, T. E.; Offenberg, J. H.; Ma, P. K.; Jimenez, J. L. Modeling the Formation and Aging of Secondary Organic Aerosols in Los Angeles during CalNex 2010. *Atmospheric Chemistry and Physics* **2015**. <https://doi.org/10.5194/acp-15-5773-2015>.
- (51) Pierce, J. R.; Engelhart, G. J.; Hildebrandt, L. Constraining Particle Evolution from Wall Losses, Coagulation, and Condensation-Evaporation in Smog-Chamber Experiments: Optimal Estimation Based on Size .... *Aerosol Sci. Technol.* **2008**.
- (52) Zawadowicz, M. A.; Lee, B. H.; Shrivastava, M.; Zelenyuk, A.; Zaveri, R. A.; Flynn, C.; Thornton, J. A.; Shilling, J. E. Photolysis Controls Atmospheric Budgets of Biogenic Secondary Organic Aerosol. *Environ. Sci. Technol.* **2020**, *54* (7), 3861–3870.
- (53) Chacon-Madrid, H. J.; Presto, A. A.; Donahue, N. M. Functionalization vs. Fragmentation: N-Aldehyde Oxidation Mechanisms and Secondary Organic Aerosol Formation. *Phys. Chem. Chem. Phys.* **2010**, *12* (42), 13975–13982.
- (54) He, Y.; Akherati, A.; Nah, T.; Ng, N. L.; Garofalo, L. A.; Farmer, D. K.; Shiraiwa, M.; Zaveri, R. A.; Cappa, C. D.; Pierce, J. R.; Jathar, S. H. Particle Size Distribution Dynamics Can Help Constrain the Phase State of Secondary Organic Aerosol. *Environ. Sci. Technol.* **2021**, *55* (3), 1466–1476.
- (55) Nah, T.; Sanchez, J.; Boyd, C. M.; Ng, N. L. Photochemical Aging of  $\alpha$ -Pinene and  $\beta$ -Pinene Secondary Organic Aerosol Formed from Nitrate Radical Oxidation. *Environ. Sci. Technol.* **2016**, *50* (1), 222–231.
- (56) Canagaratna, M. R.; Jimenez, J. L.; Kroll, J. H.; Chen, Q.; Kessler, S. H.; Massoli, P.; Hildebrandt Ruiz, L.; Fortner, E.; Williams, L. R.; Wilson, K. R.; Surratt, J. D.; Donahue, N. M.; Jayne, J. T.; Worsnop, D. R. Elemental Ratio Measurements of Organic Compounds Using Aerosol Mass Spectrometry: Characterization, Improved Calibration, and Implications. *Atmospheric Chemistry and Physics* **2015**. <https://doi.org/10.5194/acp-15-253-2015>.
- (57) Tkacik, D. S.; Presto, A. A.; Donahue, N. M.; Robinson, A. L. Secondary Organic Aerosol Formation from Intermediate-Volatility Organic Compounds: Cyclic, Linear, and Branched Alkanes. *Environ. Sci. Technol.* **2012**, *46* (16), 8773–8781.
- (58) Kroll, J. H.; Donahue, N. M.; Jimenez, J. L.; Kessler, S. H.; Canagaratna, M. R.; Wilson, K. R.; Altieri, K. E.; Mazzoleni, L. R.; Wozniak, A. S.; Bluhm, H.; Mysak, E. R.; Smith, J. D.; Kolb, C. E.; Worsnop, D. R. Carbon Oxidation State as a Metric for Describing the Chemistry of Atmospheric Organic Aerosol. *Nat. Chem.* **2011**, *3* (2), 133–139.
- (59) Chacon-Madrid, H. J.; Donahue, N. M. Fragmentation vs. Functionalization: Chemical Aging and Organic Aerosol Formation. *Atmos. Chem. Phys.* **2011**.
- (60) Loza, C. L.; Craven, J. S.; Yee, L. D.; Coggon, M. M.; Schwantes, R. H.; Shiraiwa, M.; Zhang, X.;

- Schilling, K. A.; Ng, N. L.; Canagaratna, M. R.; Ziemann, P. J.; Flagan, R. C.; Seinfeld, J. H. Secondary Organic Aerosol Yields of 12-Carbon Alkanes. *Atmos. Chem. Phys.* **2014**, *14* (3), 1423–1439.
- (61) Chhabra, P. S.; Flagan, R. C. Elemental Analysis of Chamber Organic Aerosol Using an Aerodyne High-Resolution Aerosol Mass Spectrometer. *Chemistry and Physics* **2010**.
- (62) Song, C.; Na, K.; Warren, B.; Malloy, Q.; Cocker, D. R., 3rd. Impact of Propene on Secondary Organic Aerosol Formation from M-Xylene. *Environ. Sci. Technol.* **2007**, *41* (20), 6990–6995.
- (63) Chan, A. W. H.; Chan, M. N.; Surratt, J. D.; Chhabra, P. S.; Loza, C. L.; Crouse, J. D.; Yee, L. D.; Flagan, R. C.; Wennberg, P. O.; Seinfeld, J. H. Role of Aldehyde Chemistry and NO<sub>x</sub> Concentrations in Secondary Organic Aerosol Formation. *Atmos. Chem. Phys.* **2010**, *10* (15), 7169–7188.
- (64) Yee, L. D.; Kautzman, K. E.; Loza, C. L.; Schilling, K. A.; Coggon, M. M.; Chhabra, P. S.; Chan, M. N.; Chan, A. W. H.; Hersey, S. P.; Crouse, J. D.; Wennberg, P. O.; Flagan, R. C.; Seinfeld, J. H. Secondary Organic Aerosol Formation from Biomass Burning Intermediates: Phenol and Methoxyphenols. *Atmos. Chem. Phys.* **2013**, *13* (16), 8019–8043.
- (65) Hurley, J. F.; Smiley, E.; Isaacman-VanWertz, G. Modeled Emission of Hydroxyl and Ozone Reactivity from Evaporation of Fragrance Mixtures. *Environ. Sci. Technol.* **2021**, *55* (23), 15672–15679.
- (66) Jathar, S. H.; Gordon, T. D.; Hennigan, C. J.; Pye, H. O. T.; Pouliot, G.; Adams, P. J.; Donahue, N. M.; Robinson, A. L. Unspeciated Organic Emissions from Combustion Sources and Their Influence on the Secondary Organic Aerosol Budget in the United States. *Proc. Natl. Acad. Sci. U. S. A.* **2014**, *111* (29), 10473–10478.
- (67) O'Donnell, Samuel, Ali Akherati, Yicong He, Anna L. Hodshire, John E. Shilling, Chongai Kuang, Jerome D. Fast, Fan Mei, Siegfried Schobesberger, Joel A. Thornton, James N. Smith, Shantanu H. Jathar, and Jeffrey R. Pierce: Look up: Probing the vertical profile of new particle formation and growth in the planetary boundary layer with models and observations. *J. Geophys. Res.*, In Prep.
- (68) Chu, B.; Chen, T.; Liu, Y.; Ma, Q.; Mu, Y.; Wang, Y.; Ma, J.; Zhang, P.; Liu, J.; Liu, C.; Gui, H.; Hu, R.; Hu, B.; Wang, X.; Wang, Y.; Liu, J.; Xie, P.; Chen, J.; Liu, Q.; Jiang, J.; Li, J.; He, K.; Liu, W.; Jiang, G.; Hao, J.; He, H. Application of Smog Chambers in Atmospheric Process Studies. *Natl Sci Rev* **2021**, *9* (2), nwab103.
- (69) Wang, N.; Jorga, S. D.; Pierce, J. R.; Donahue, N. M.; Pandis, S. N. Particle Wall-Loss Correction Methods in Smog Chamber Experiments. *Atmos. Meas. Tech.* **2018**, *11* (12), 6577–6588.
- (70) Krechmer, J. E.; Day, D. A.; Jimenez, J. L. Always Lost but Never Forgotten: Gas-Phase Wall Losses Are Important in All Teflon Environmental Chambers. *Environ. Sci. Technol.* **2020**, *54* (20), 12890–12897.
- (71) Palm, B. B.; Campuzano-Jost, P.; Ortega, A. M. In Situ Secondary Organic Aerosol Formation from Ambient Pine Forest Air Using an Oxidation Flow Reactor. *Atmospheric* **2016**.
- (72) Chen, D.; Li, Q.; Stutz, J.; Mao, Y.; Zhang, L.; Pikel'naya, O.; Tsai, J. Y.; Haman, C.; Lefer, B.; Rappenglück, B.; Alvarez, S. L.; Neuman, J. A.; Flynn, J.; Roberts, J. M.; Nowak, J. B.; de Gouw, J.; Holloway, J.; Wagner, N. L.; Veres, P.; Brown, S. S.; Ryerson, T. B.; Warneke, C.; Pollack, I. B. WRF-Chem Simulation of NO<sub>x</sub> and O<sub>3</sub> in the L.A. Basin during CalNex-2010. *Atmos. Environ.* **2013**, *81*, 421–432.

## SUPPLEMENTARY INFORMATION

**S1:** The SOA mass yields for the OVOCs studied in this work were based on the SOA parameters listed in Table 2. The SOA mass yields for the following VOCs were based on parameters determined in previous work: *n*-dodecane, methylundecane, hexylcyclohexane, isoprene,  $\alpha$ -pinene, limonene,  $\beta$ -caryophyllene, benzene, toluene, *m*-xylene, *o*-xylene, naphthalene, alkylfuran mixture (2-methylfuran and dimethylfuran), phenol, guaiacol, and syringol.<sup>1,2,3</sup> For the remaining VOCs, the following surrogate assignments were made to calculate SOA formation: linear alkanes - *n*-dodecane, branched alkanes - methylundecane, cyclic alkanes - hexylcyclohexane, alkenes (C<sub>5</sub> to C<sub>9</sub>) - isoprene, alkenes (C<sub>10+</sub>) -  $\alpha$ -pinene, single-ring aromatics (C<sub>8+</sub>) - *m*-xylene, multi-ring aromatics - naphthalene, gasoline IVOCs - C<sub>13</sub> linear alkane, diesel IVOCs - C<sub>15</sub> linear alkane, furans - alkylfuran mixture, oxygenated aromatics - phenol/guaiacol, glycol ethers - diethylene glycol, and acetates and esters - Texanol. We should point out that the SOM-TOMAS parameters inform the trajectory of the VOC and its oxidation products through a carbon-oxygen grid subject to functionalization and fragmentation reactions. By definition, then, the SOA mass yields for a precursor, with a different carbon and oxygen number than the assigned surrogate, will be different from those for the surrogate. We deliberately chose a low SOA mass yield surrogate for glycol ethers (i.e., diethylene glycol instead of carbitol or butyl carbitol) and acetates and esters (i.e., Texanol instead of methyl palmitate, DPGMEA, or dimethyl glutarate) to provide a lower bound on the SOA production estimate from VCP VOCs.

**S2:** Results for SoCAB are shown in Figure S3 and, despite the use of a coarser emissions inventory, the findings were generally consistent with those presented earlier for NYC. VOC emissions from VCP use ( $11.4 \text{ kg person}^{-1} \text{ yr}^{-1}$ ) were  $1.6\times$  of those from mobile sources ( $7.3 \text{ kg person}^{-1} \text{ yr}^{-1}$ ); compared to NYC, SoCAB had higher evaporative gasoline emissions presumably from a warmer climate and higher diesel exhaust emissions from a larger footprint of on- and off-road diesel vehicles. SOA production from VCP use ( $0.38 \text{ kg person}^{-1} \text{ yr}^{-1}$ ) was  $2.6\times$  that from mobile sources ( $0.15 \text{ kg person}^{-1} \text{ yr}^{-1}$ ), which was nearly identical to that in NYC. The precursor contributions to VCP SOA were very similar between SoCAB and NYC with nine VOCs (out of fifteen) overlapping between the two regions. Similarities between SoCAB and NYC can partly be attributed to similar methodologies being used to develop those respective emissions inventories.

Table S1: Summary of data for the high NO<sub>x</sub> chamber experiments performed by Li et al.<sup>18</sup> and those used in this work to test SOA parameters for select OVOCs.

VCP OVOC	Formula	MW (g.mole <sup>-1</sup> )	k <sub>OH</sub> (cm <sup>3</sup> molec <sup>-1</sup> s <sup>-1</sup> )	Seed (μm <sup>2</sup> cm <sup>-3</sup> )	Surrogate VOC Mix.?	H <sub>2</sub> O <sub>2</sub> Added	Initial VOC <sub>0</sub> (ppbv)	Initial NO (ppbv)	Initial NO <sub>2</sub> (ppbv)	OH Exposure (molec.hr cm <sup>-3</sup> )	Max. SOA (μg m <sup>-3</sup> )	SOA Mass Yield (Max.)	SOA O:C
Propylene Glycol	C <sub>3</sub> H <sub>8</sub> O <sub>2</sub>	76.09	2.15×10 <sup>-11</sup>	249	Y	N	40	17	6.4	1.04×10 <sup>7</sup>	6.22	0.09	0.55 <sup>&amp;</sup>
Diethylene Glycol	C <sub>4</sub> H <sub>10</sub> O <sub>3</sub>	106.12	2.75×10 <sup>-11</sup>	NA	Y	N	80	20	13	9.80×10 <sup>6</sup>	3.44	0.02	NM
Carbitol	C <sub>6</sub> H <sub>14</sub> O <sub>3</sub>	134.17	5.16×10 <sup>-11</sup>	NA	Y	Y	40	7.6	22	1.52×10 <sup>7</sup>	25.57	0.12	0.6-1.2 <sup>&amp;</sup>

<sup>&</sup>Measurement based on a different experiment; NA=unseeded experiment; NM=not measured.

Table S2: Top 50 VOCs contributing to VCP SOA in NYC.

Species	Contribution to VCP SOA (%)
Fragrances	25.8
Propylene glycol	8.9
C13-C18 mixed hydrocarbons	5.4
Isopropyl palmitate	5.0
C12 cycloalkanes	2.6
Glycerol	2.6
Xylenes	2.5
C12 branched alkanes	2.5
C11 cycloalkanes	2.4
C16 branched alkanes	2.0
N,N-Diethyl-m-Toluamide and Isomers	1.8
C13 branched alkanes	1.7
C15 cycloalkanes	1.7
C17 branched alkanes	1.6
Butyl carbitol	1.5
n-dodecane	1.4
Pine oil	1.3
C11 branched alkanes	1.2
n-undecane	1.2
C9 cycloalkanes	1.2
C16 cycloalkanes	1.1
C10 cycloalkanes	1.1
n-pentadecane	1.0
dipropylene glycol monobutyl ether	1.0
Ethylene glycol phenyl ether	1.0
Dipropylene glycol	0.9
C15 branched alkanes	0.9
C10 branched alkanes	0.9
C10 disubstituted benzenes	0.7
Butyl cellosolve (2-butoxyethanol) (egbe)	0.7
n-hexadecane	0.7

2,2,4-trimethyl-1,3-pentanediol isobutyrate (Texanol)	0.7
Toluene	0.7
C8 cycloalkanes	0.7
C13 cycloalkanes	0.6
C14 cycloalkanes	0.6
D-limonene (4-isopropenyl-1-methylcyclohexane)	0.6
C16-C18 alkyl methyl esters	0.5
C10 internal alkenes	0.5
Propylene glycol butyl ether (1-butoxy-2-propanol)	0.5
n-nonane	0.4
C10 alkyl phenols	0.4
n-tetradecane	0.3
Ethylbenzene	0.3
n-tridecane	0.3
Hexylene glycol (2-methyl-2,4-pentanediol)	0.3
1,2,4-trimethylbenzene	0.3
C11 internal alkenes	0.3
C15 naphthalenes	0.3
Diethylene glycol	0.3

Table S3: Top 50 VOCs contributing to VCP SOA in SoCAB.

Species	Contribution to VCP SOA (%)
Fragrances	16.8
Oxygenated IVOCs	10.7
Diesel	5.4
IVOCs	5.4
Propylene glycol	4.9
Pine Oil	4.5
Xylenes	3.6
C16 branched alkanes	2.5
C15 cycloalkanes	2.5
Limonene	2.3
C12 branched alkanes	2.1
C17 branched alkanes	1.9
Butyl carbitol	1.9
C12 cycloalkanes	1.8
Carbitol	1.7
C11 cycloalkanes	1.6
C16 cycloalkanes	1.6
toluene	1.5
C13 branched alkanes	1.4
n-pentadecane	1.3
n-dodecane	1.2
C15 branched alkanes	1.1
C9 cycloalkanes	1.1
n-undecane	1.0
n-hexadecane	0.9
i-butyl acetate	0.9
C14 cycloalkanes	0.9
n-butyl acetate	0.8
C8 cycloalkanes	0.8
C11 branched alkanes	0.8
Hexylene glycol	0.8

C10 cycloalkanes	0.6
C10 branched alkanes	0.6
2-Butoxyethanol	0.5
Dipropylene glycol Methyl Ether	0.5
Texanol	0.5
C10 disubstituted benzenes	0.5
n-tetradecane	0.5
n-nonane	0.4
C11 trisubstituted benzenes	0.4
C12 trisubstituted benzenes	0.4
Phenoxyethanol	0.4
C13 cycloalkanes	0.4
Dipropylene glycol	0.3
Ethylbenzene	0.3
C14 naphthalenes	0.3
C10 trisubstituted benzenes	0.3
C9 branched alkanes	0.3
1,2,4-trimethylbenzene	0.3
n-octane	0.3

Table S4: Top 50 VOCs contributing to VCP SOA in the US

Species	Contribution to VCP SOA (%)
C16-C18 alkyl methyl esters	14.9
C14-C16 alkanes	6.3
Butyl carbitol	5.9
Terpene	4.4
Propylene glycol	4.4
Limonene	3.7
Xylenes	3.3
C12 cycloalkanes	3.1
C12 branched alkanes	2.8
C11 cycloalkanes	2.8
N,N-diethyl-m-toluamide	2.5
Carbitol	2.4
Toluene	2.2
C13 branched alkanes	2.1
Ethylene glycol monobutyl ether	1.9
n-dodecane	1.7
Misc. esters	1.6
n-undecane	1.5
DL-limonene (dipentene)	1.4
Phenoxyethanol	1.4
Texanol	1.2
Glycol ether dpnb	1.1
Dipropylene glycol methyl ether acetate	0.9
1-butoxy-2-propanol	0.9
C15 cycloalkanes	0.7
C16 branched alkanes	0.7
Styrene	0.7
Methyl propylcyclohexanes	0.6
C10 internal alkenes	0.6
C11 branched alkanes	0.6
Isomers Of undecane	0.6

C13 cycloalkanes	0.6
Dipropylene glycol monomethyl ether	0.6
C17 branched alkanes	0.6
C10 alkylphenols	0.5
Isomers Of decane	0.5
C16 cycloalkanes	0.4
C11 internal alkenes	0.4
C10 cycloalkanes	0.4
Benzyl alcohol	0.4
n-tridecane	0.4
n-pentadecane	0.4
C11 trialkyl benzenes	0.4
2-ethylhexyl benzoate	0.3
Citrus terpenes	0.3
2-methyldecane	0.3
Ethylmethylcyclohexanes	0.3
C15 branched alkanes	0.3
UNC peaks to CBM xylene	0.3
n-decane	0.3

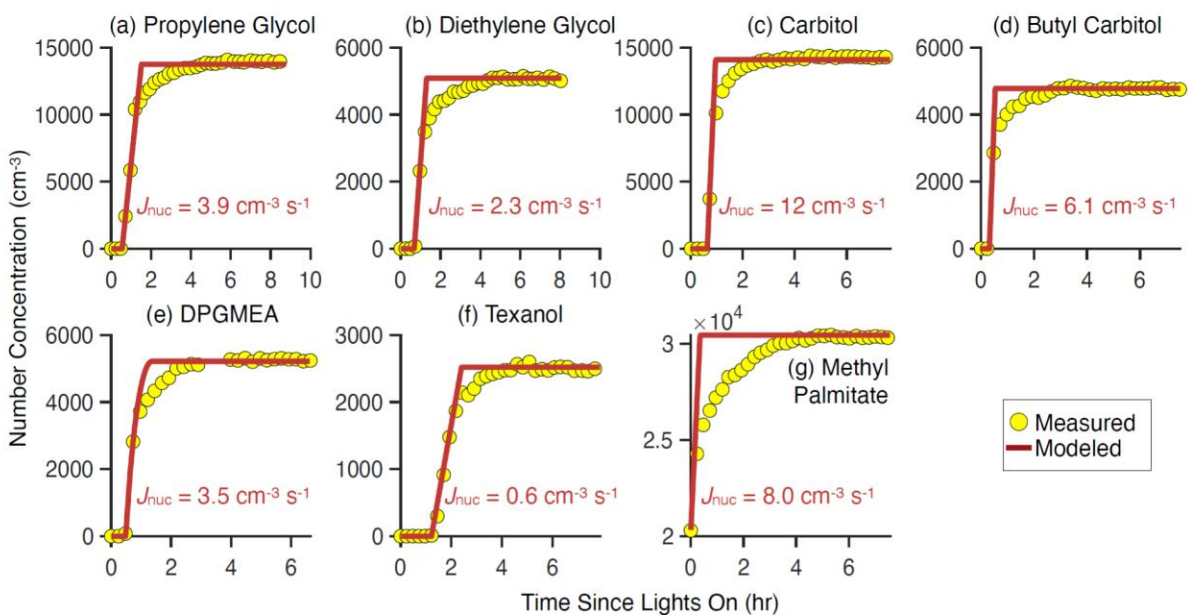


Figure S1: (a-f) Modeled and measured total particle number concentration in experiments where ammonium sulfate seed was not added to the chamber and SOA was allowed to nucleate. (g) Modeled and measured total particle number concentration for the methyl palmitate experiment, where a small amount of nucleation was observed. For simplicity, a constant nucleation rate was determined by fitting the initial increase in the particle number concentration and nucleation was turned off after reaching the peak number concentration.

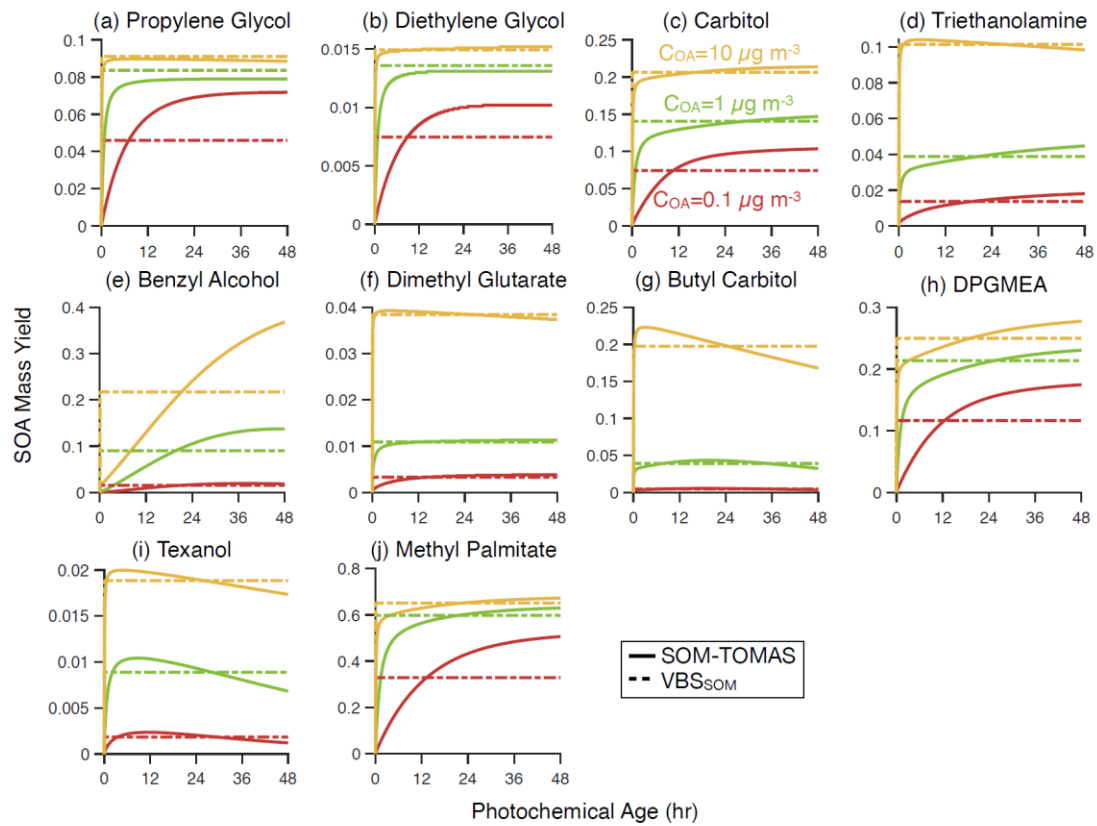


Figure S2: Same as Figure 6 but for OVOCS studied in this work. Results for carbitol, shown in Figure 6, are repeated in this figure.

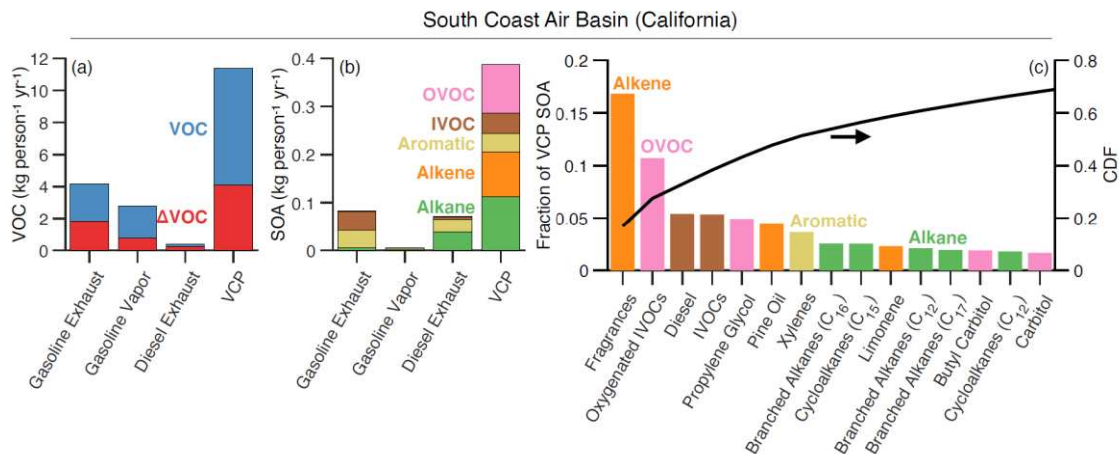


Figure S3: Same as Figure 8 but for the South Coast Air Basin (SoCAB).